Techno-economic assessment of the horizontal geothermal heat pump systems: A comprehensive review

Yuanlong Cui [a, b], Jie Zhu [a *], Ssennoga Twaha [a], Junze Chu [a], Hongyu Bai [a], Kuo Huang [a], Xiangjie Chen [a], Stamatis Zoras [b], Zohreh Soleimani [b]

[a] Department of Architecture and Built Environment, University of Nottingham, Nottingham NG7 2RD, United Kingdom

[b] Department of Built Environment, College of Engineering and Technology, University of Derby, Derby DE22 3AW, UK

Contents

* Corresponding author. Tel: +44-115-8466141 Fax: +44-115-951315
E-mail address: jie.zhu@nottingham.ac.uk

Abstract

Geothermal heat pump has been widely recognized as one of the promising technologies for building applications because of its high energy efficiency and low operating expense, however the high capital investment and installation costs discourage building owners to choose such a system. The horizontal geothermal heat pump system with reduced cost is a viable option that would be utilized widely, the aim of this paper is to catalogue and critique a range of effective approaches for the horizontal geothermal heat pump systems in different regions based on techno-economic assessment data. A ground heat exchanger is a vital component of the horizontal geothermal heat pump. The state-of-the-art analytical and numerical models of the linear-loop, slinky-coil and spiral-coil ground heat exchangers are generalized, in addition to their advantages and disadvantages. A large number of economic evaluation methods for analysing the financial performance of the horizontal geothermal heat pump system are presented. At the end, the standpoints, recommendations and potential future study on the horizontal geothermal heat pump system are deliberated.

Keywords: Horizontal geothermal heat pump, Ground heat exchanger, Analytical models, Numerical models, Economic evaluation approaches

1. Introduction

A great majority of the worldwide energy is consumed for space heating/cooling and electricity generation, with the plurality coming from fossil fuels [1]. The utilization of fossil fuels is destructive to the environment due to greenhouse gases emission, which has been identified as the major contributor to the climate change [2, 3]. To attack the climate change, it is significant to develop alternative energy technologies like solar [4], wind [5], biomass [6] and geothermal energy [7, 8], which are able to provide energy in more efficient and healthy way. In this context, geothermal heat pump (GHP) system has already turned into a dominant choice for energy supply in commercial and residential buildings owing to its high Coefficient of Performance (COP) [9]. The global GHP capacity is anticipated to increase by about 150% from 2013 to 2020 [10], as shown in Fig.1.

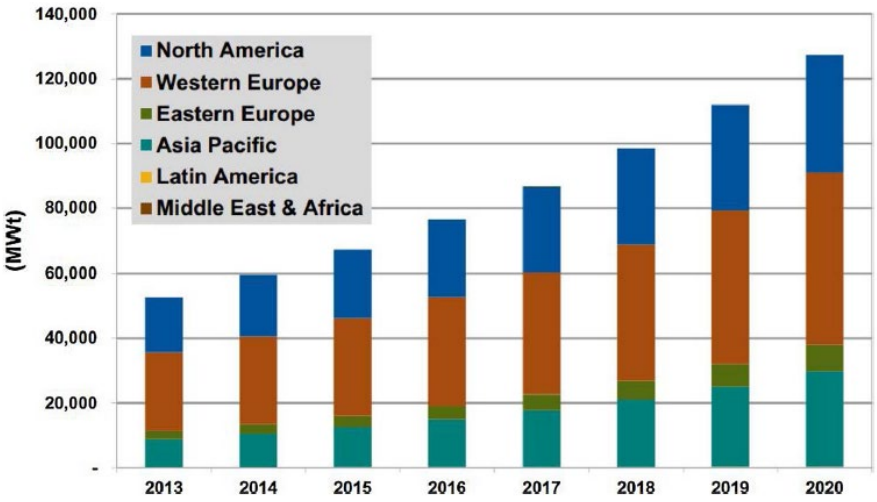

Fig. 1. World installed and predicted capacity of GHP units from 2013 to 2020 [10]

In comparison to other traditional heating and cooling units, the GHP system has a lower operating cost and less influence on the atmosphere [11, 12]. Soil temperature is normally lower than the ambient air temperature in cooling season, but higher in heating season. As a result, the GHP system makes use of the soil as a heat source in heating season, and as a heat sink in cooling season. In general, a GHP system composes of three major elements: ground heat exchanger (GHE), heat pump and heat distribution subsystem as given in Fig. 2.

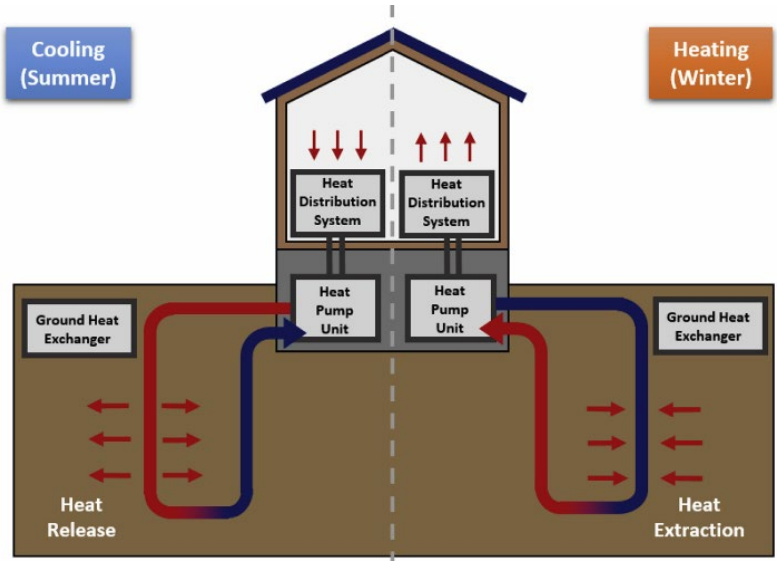

Fig. 2. Schematic of GHP system for space heating and cooling [13]

Moreover, the GHP system is divided into open-loop and closed-loop types, and extracts/rejects thermal energy from/to soil via circulating a working fluid within the GHE [13, 14]. Two popular closed-loop ground loops are utilized in the GHEs: vertical and horizontal types. Specifically, the vertical GHE requires approximately 50-150 m deep holes in the soil, and its main configurations include the U-tube, concentric tube and pile heat exchangers. In comparison, the horizontal GHE can be installed in shallow horizontal trenches 1-2 m deep, and its typical configurations are the linear-loop, spiral-coil and slinky-coil heat

exchangers [15, 16]. Furthermore, the installation of the vertical GHE is expensive compared with that of the horizontal GHE, but the horizontal GHE needs the large land area [17, 18]. Notably, in recent years, researches into the horizontal GHE focus on analytical and numerical models, system performance and behaviour of energy storage for various loop configurations and working conditions [19, 20].

The application of the GHP system for space heating and cooling has been improved in recent years, it is predicted that this trend will carry on in the next decades [21, 22]. Notably, the geothermal energy is less influenced by weather condition than other renewable energies like wind and solar [23].

There are many techno-economic studies on the horizontal GHP system with diverse scenarios. Hence, lots of economic performance indicators are used to analyze the GHP finical benefits, such as Life Cycle Cost (LCC) , Levelized Cost of Heat (LCOH) , Levelized Cost of Service (LCOS) , Net Present Value (NPV) , Bin method , Capital Recovery Factor (CRF) , Present Worth (PW) , Annual Worth (AW) , Discounted Cash Flow Analysis (DCFA) [34], Internal Rate of Return (IRR) , Simple Payback Period (SPP) and Discounted Payback Period (DPP) approaches. But there is still a research gap in the light of generalizing the techno-economic solutions to evaluate technical and economic factors that influence the horizontal GHP system design and performance. The economic feasibility of a GHP system heavily depends on the capital and installation expenses of the GHE. Therefore, the aim of this study is to fill this research gap by offering not only an overall review but also a systematic summary of analytical, numerical and economic models for the horizontal GHP. Moreover, this work improves the awareness of different methodologies and hypotheses for these models, along with their major advantages and disadvantages. Additionally, the alternative methods, recommendations and future studies are illustrated as well. In the meantime, the vital demands for comparing the economic indicators in financial analysis for the horizontal GHP system are identified including LCC, LCOH, LCOS, NPV, Bin method, CRF, PW, DCFA, IRR, SPP and DPP. At the end, the summaries of the techno-economic solutions are produced in choosing an appropriate model for predicting the system energy output, efficiency, economic benefit, return on investment and payback time. This paper is presented in the following structure: a brief background concerning different types of the horizontal GHP system is introduced in Section 2, the technical and economic approaches are illustrated and generalized in Section 3, the challenges of the horizontal GHP system and suggestions for future study are given in Section 4, the important conclusions are summarized in Section 5.

2. Types of the horizontal GHE

The horizontal GHE has been extensively applied in the GHP system in several regions of the world. Thermal performance of the horizontal GHP system is comparatively lower than the vertical GHP system's owing to the seasonal soil temperature variation, thereby the horizontal GHP system needs larger land area and longer pipe. However, the horizontal GHE is able to offer a cost-effective option as the excavation expense of horizontal trench is much lower than the vertical installation cost. The

horizontal GHE is classified into three styles including linear, slinky-coil and spiral-coil arrangements as shown in Fig. 3. The spiral and slinky configurations have higher heat transfer rates per trench unit length [24].

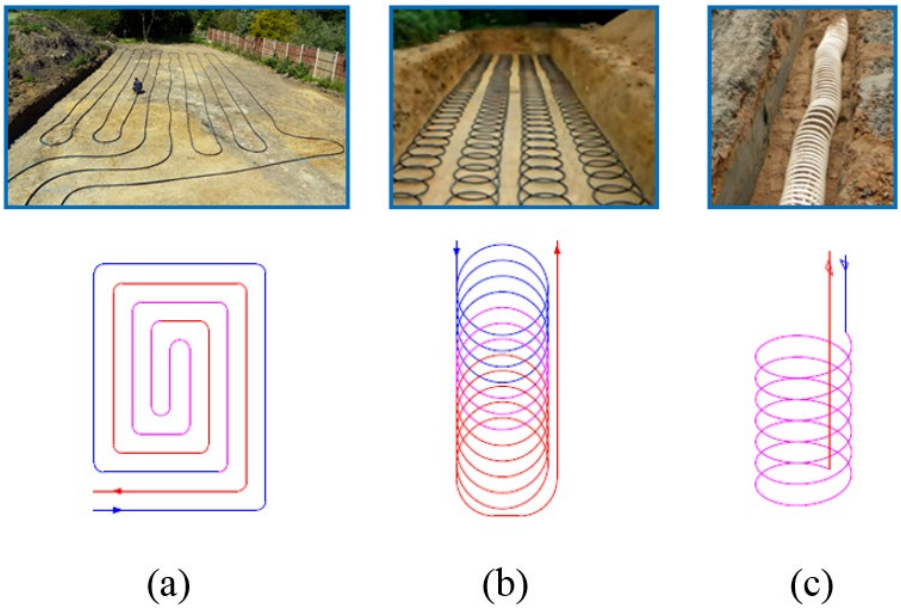

Fig. 3. Horizontal closed GHEs: (a) linear-loop; (b) slinky-coil; (c) spiral-coil [24]

2.1 Linear-loop GHEs

In term of the closed-loop system with sufficient ground area, the ground loop is arranged horizontally underneath the surface of ground within backfilled trenches. Three basic configurations including the trench, series and parallel loops, are presented in Fig.4. Their arrangements mainly rely on land availability and heat transfer demand. The series and parallel layouts typically require smaller land regions. Moreover, the series and parallel loops are able to be combined, improving the flexible horizontal fittings. The horizontal GHP systems are generally more cost-effective than vertical types for installations, on the basis of lower expenses in comparison to drilling [24, 25]. And the horizontal linear loops are laid and buried typically 1–2 m below ground surface [25].

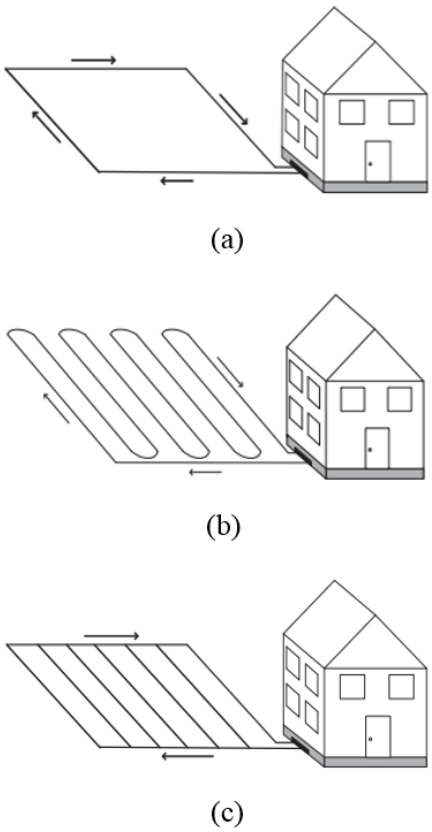

Fig. 4. Schematic of linear GHEs: (a) trench configuration loop; (b) series loop; (c) parallel loop [25]

2.2 Slinky-coil GHEs

To make full use of available land area for trenching, the horizontal GHE can be installed as slinky loops that are positioned either horizontally or vertically as presented in Fig. 5.

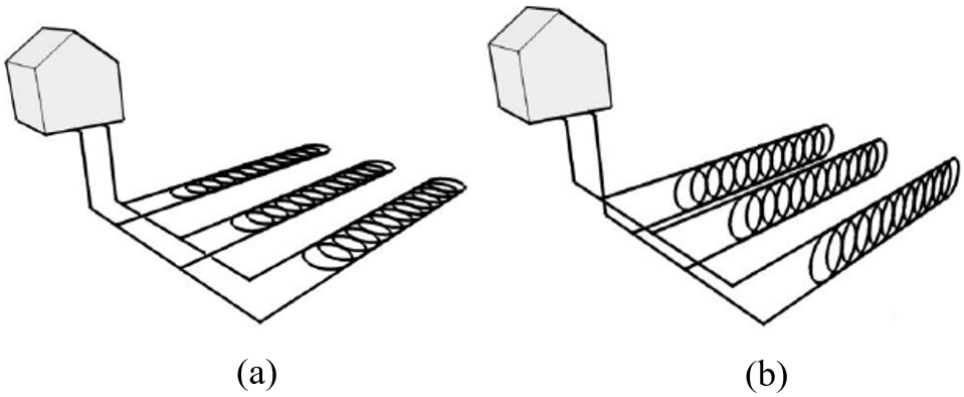

Fig. 5. Schematic of horizontal slinky GHEs: (a) horizontal; (b) vertical [25, 26]

The slinky GHE is typically sited vertically in the narrow trench when the excavation is made with a trenching machine. On the contrary, normally mounted horizontally [26]. The long pipe increases circulation pump work thus lowering the system COP. Loop pitch is the distance between two slinky coils and typically in the range of 0.6–1.2 m [25]. For the slinky GHE, the width

of trench ranges 0.8–1.8 m with separation distance in multiple trenches of 2–4 m [25]. The loops sit in upright position in narrower trench generally with 15-20 cm wide [25]. Narrower trench requirement in vertical layout could reduce the total installation cost.

2.3 Spiral-coil GHEs

Spiral loop layouts are similar to the slinky-loops', because they are normally horizontally oriented in shallow trenches as given in Fig. 6.

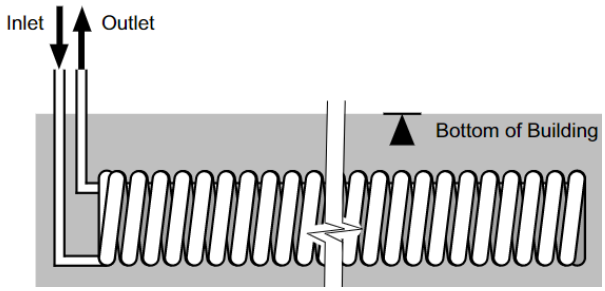

Fig. 6. Schematic of horizontal spiral-coil GHE [27]

Nonetheless, the piping is arranged within circular loops in the trench [28]. The spiral loops need less regions than traditional loops and have lower trenching demands, however, they require greater piping length for a fixed load [28]. The main merit of the spiral-loop arrangement is the decreased horizontal region demand, which permits diverse trenching equipment to be utilized, sometimes producing beneficial economics [29, 30]. An optimal design condition concerning coil pitch and setting depth are 0.08 m and 2.5 m, respectively [29, 31].

3. Techno-economic models

3.1 Technical models

Nowadays, technical models are still an important domain for research. They have been regarded as essential implements for long time performance assessment, energy output and system optimisation. In fact, heat transfer analysis inside a horizontal GHE contains several uncertain factors as illustrated in Fig. 7, for example installation depth, working fluid rate, thermal conductivity of the soil and pitch spiral diameter [32].

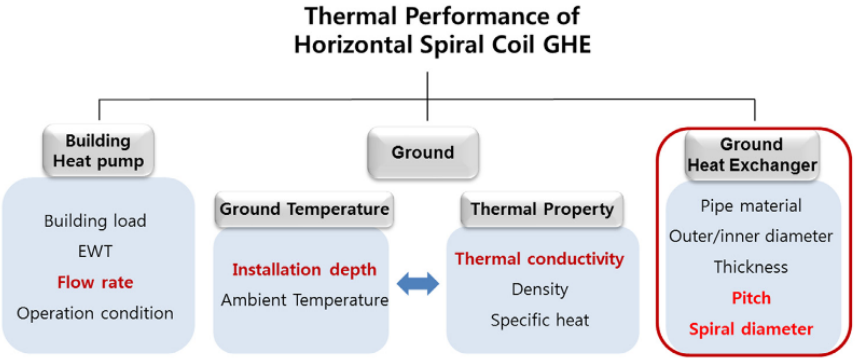

Fig. 7. The impact factors of thermal performance of horizontal spiral-coil GHE [32]

Because of this reason, the physical process of heat transfer within the GHE is quite complex and typically divided into two parts. One part is the ground region, whereas another part is the GHE region containing the refrigerant within the pipe and buried pipes. At present, many prevalent analytical and numerical models are used in the process of heat transfer analysis in the horizontal GHE through involving linear-loop GHE , slinky-coil GHE and spiral-coil GHE models. These analytical and numerical models are illustrated in the following section.

3.1.1 Linear-loop GHE models

Kupiec et al. [18] setup one-dimensional transient heat transfer model for the horizontal linear GHE to assess the system performance. Fig. 8 (a) depicts the GHE as a fictitious cuboid wherein heat is produced. Temperature difference along the y-axis is analysed by means of classifying the heat exchanger into stages. A thermal fluid flows in series by the neighbouring stages, which is regarded as perfect-mixing tanks in the model. Fig. 8 (b) displays the thermal fluid flow between the upper and lower heat exchangers.

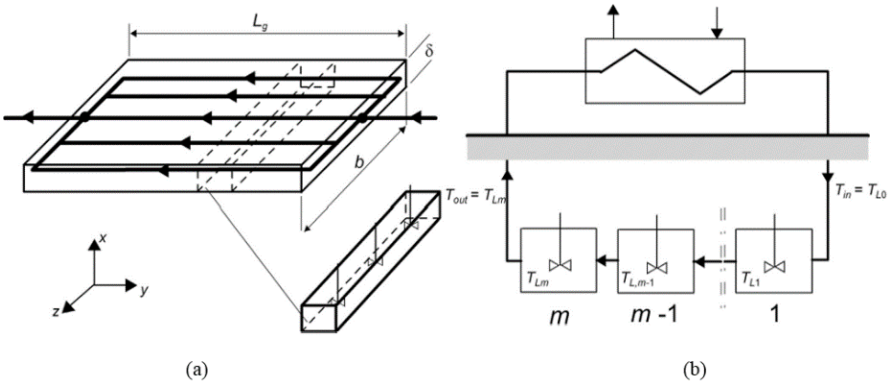

Fig. 8. Schematic of: (a) GHE as a fictitious cuboid; (b) working fluid flow within the GHE [18]

The initial condition is given as follows:

$$t = 0: \quad T = T_b + B \cdot \exp(-\frac{x}{L}) \cdot \cos[\omega(t - t_{max}) - \frac{x}{L}] \tag{1}$$

Where B is the half of the annual maximum temperature range; ω is the frequency.

The boundary condition is written as follows:

$$x = h_{inf}, \quad T = T_b \tag{2}$$

The heat transfer rate between the soil and working fluid in the j^{th} stage is given as:

$$\dot{Q}_j = \dot{m}_L c_L (T_{Lj} - T_{L,j-1}) \tag{3}$$

The total heat transfer rate within the GHE is expressed as:

$$\dot{Q} = \sum_{j=1}^{m} \dot{Q}_j \tag{4}$$

The model is validated by test data, then utilized to assess heat exchange rate of the horizontal GHE for long-term operation period. Meanwhile, it can also be used to study the effect of different process parameters on the GHE efficiency.

Li et al. [19] established a 3D heat transfer model of HGHE system to estimate the effects of soil surface boundary conditions and diurnal shading on the system performance. A schematic diagram of the HGHE system is shown in Fig. 9. Meanwhile, the basic heat transfer equations of HGHE system, soil surface boundary and shading are illustrated in Table 1. The results indicated that high building load and shallow buried depth of HGHE have significant influences on system performance, and daily variation in shading exhibits impact on outlet temperature of HGHE up to buried depth of 2.5 m.

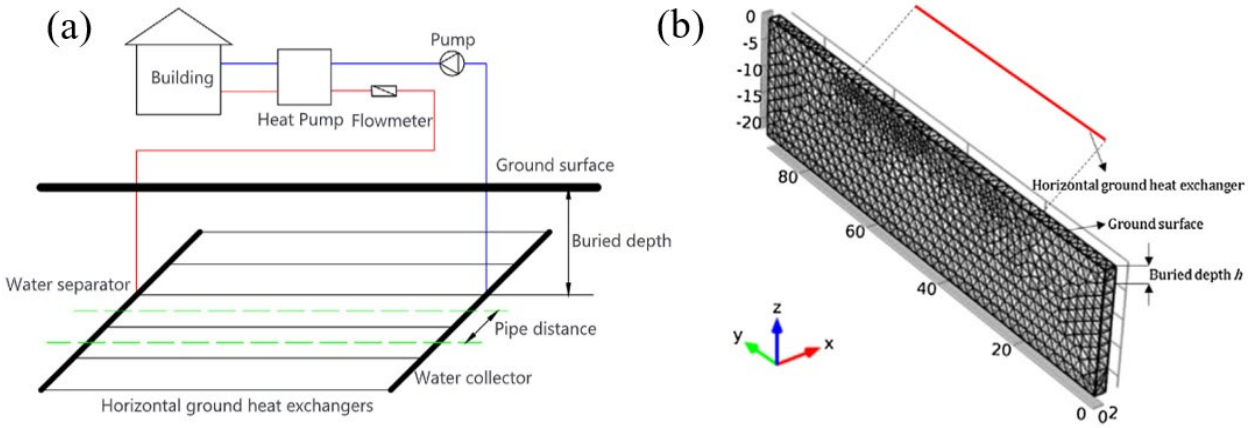

Fig. 9 (a) A typical horizontal heat pump system; (b) computational soil domain [19]

Table 1 Heat transfer equations of HGHE system [19]

Description	Equation
The working fluid flow in the HGHE:	$\rho_f A_p c_{p,f}\frac{\partial T_f}{\partial t}+\rho_f A_p c_{p,f} u\cdot\nabla T_f = A_p k_f \nabla\cdot(\nabla T_f)+\frac{1}{2}f_D\frac{\rho_f A_p}{dh}\lvert u\rvert^3+Q_{wall}$
The heat transfer between the pipe and nearby soil:	$Q_{wall}=h_{eff}(T_{ext}-T_f)$
The heat transfer in the soil:	$\rho_s c_{p,s}\frac{\partial T_s}{\partial t}=k_s\nabla\cdot(\nabla T_s)-Q_{wall}$
The soil surface boundary condition:	$-k_s\frac{\partial T_{ss}}{\partial Z}=(1-\alpha_s)R+\varepsilon_{ss}\sigma(T_{sky,K}^4-T_{ss,K}^4)+h_c(T_a-T_{ss})-E_w$
The diurnal shading	$D_{s(t)}=\frac{X_t}{W}=\frac{\cos(e-e_t)}{\tan\beta_t}\frac{H}{W}$

Pu et al. [20] investigated the effects of the five arrangements on HGHE performance by ANSYS Fluent 15.0 as shown in Fig. 10, and concluded from Fig. 11 that the heat transfer rates of U-pipe and serpentine pipe are lower than that of single pipe, which means single pipe has better thermal performance.

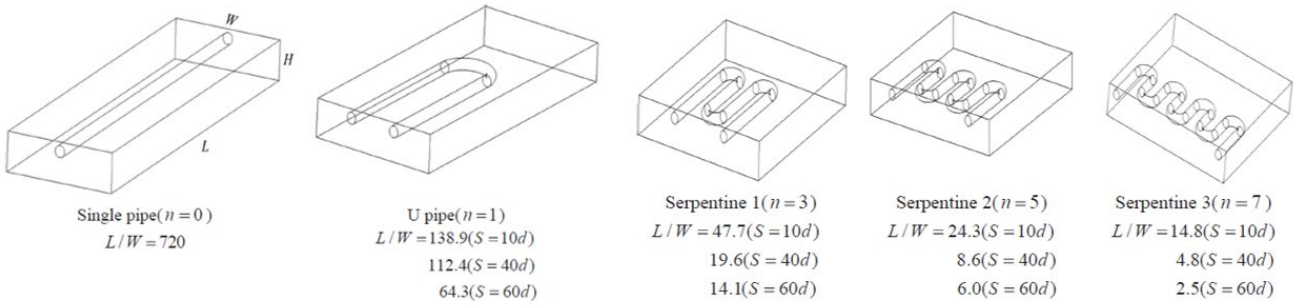

Fig. 10. Five arrangements of HGHE [20]

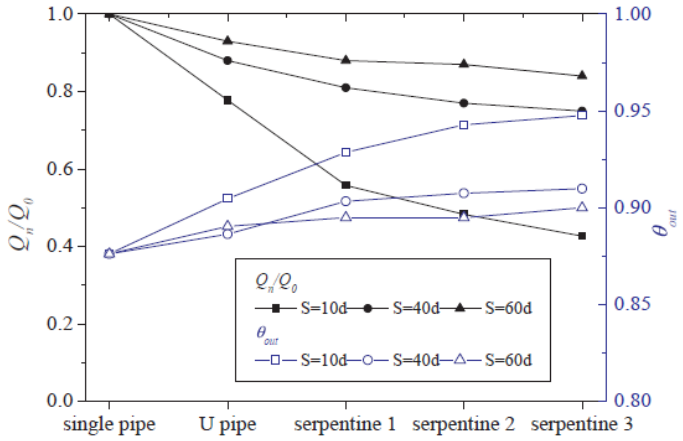

Fig. 11. The effects of five shapes arrangement of HGHE on thermal performance [20]

Meanwhile, the comparison between in-line and relative displacement of staggered pipes on the HGHE performance is presented in Fig. 12. It is found from Fig. 13 that the performance of HGHE in staggered arrangement is better than that of in-line arrangement, however, when the relative offset distance D/S ⩽ 1/3, the in-line arrangement shows a better system performance.

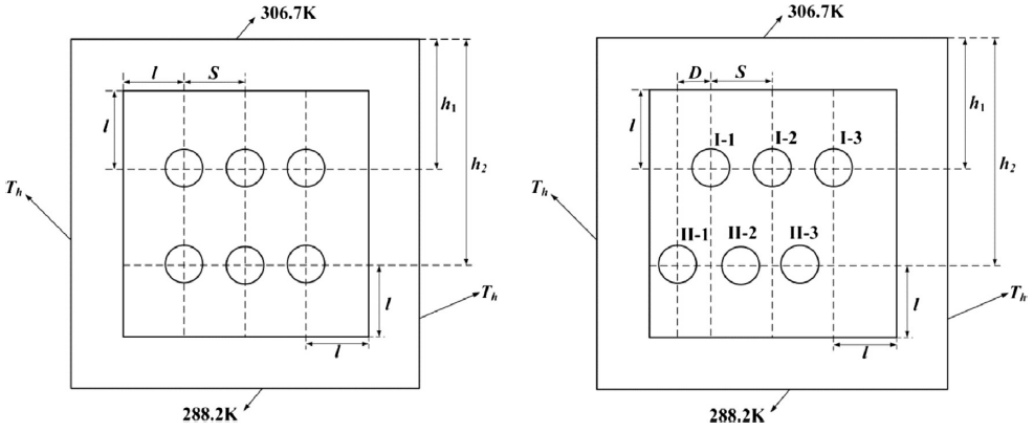

in-line arrangement staggered arrangement

Fig. 12. In-line and staggered layouts [20]

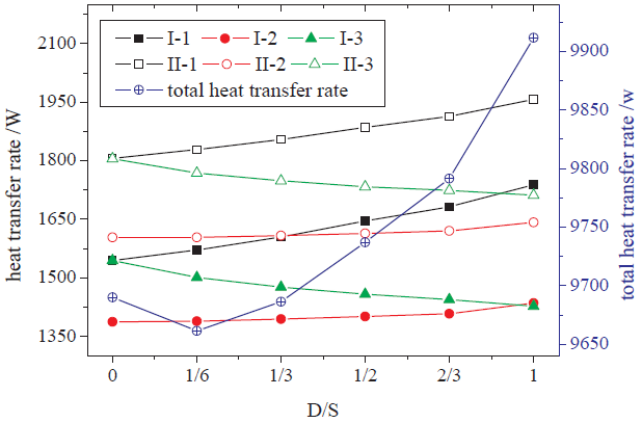

Fig. 13. The heat transfer rate vs. the offset distance [20]

Noorollahi et al. [33] studied a horizontal GHP system to fulfil a 1000 m^2 greenhouse energy demand in Iran as shown in Fig.14. To evaluate the GHP system performance, the heat transfer equations within the GHP system are given in Table 2. The heat transfer equations are resolved based on the Cranke Nicolson approach. The results demonstrate that increasing the length of GHE decreases the number of heat pumps required for the greenhouse, and also decreases the power consumption.

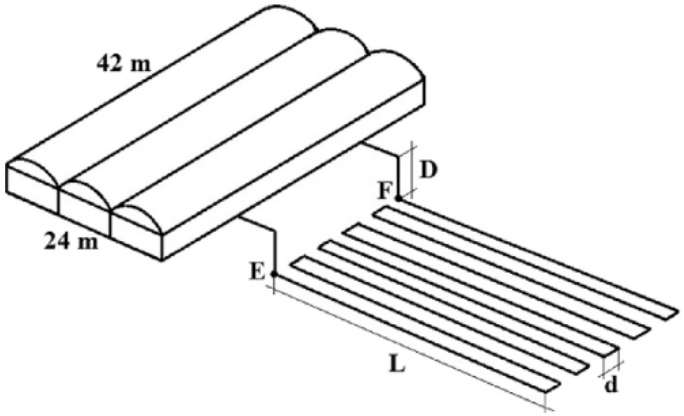

Fig. 14. The schematic of GHE system applied in the greenhouse [33]

Table 2 The heat transfer models for the greenhouse [33]

Description	Equation
The energy conservation for the greenhouse:	$mc_{air}\frac{dT}{dt} = q_{amb} + q_{sun} + q_{HP} + q_{aux}$
The heat transfer in the soil:	$\frac{\partial^2 T}{\partial r^2} + \frac{1}{r}\frac{\partial T}{\partial r} = \frac{1}{\alpha}\frac{\partial T}{\partial t}$
The heat transfer in the pipe wall:	$k_p \frac{\partial T}{\partial r}(R,t) = h[T(R,t) - T_b]$
The outlet fluid temperature:	$T_{out} = T_s + (T_{in} - T_s)\exp(-\frac{2\pi Rh}{mc_w}\Delta z)$

Todoran and Balan [34] investigated a horizontal GHP system for space heating within a small residential house as presented in Fig. 15. The basic energy balance equations are given in Table 3.

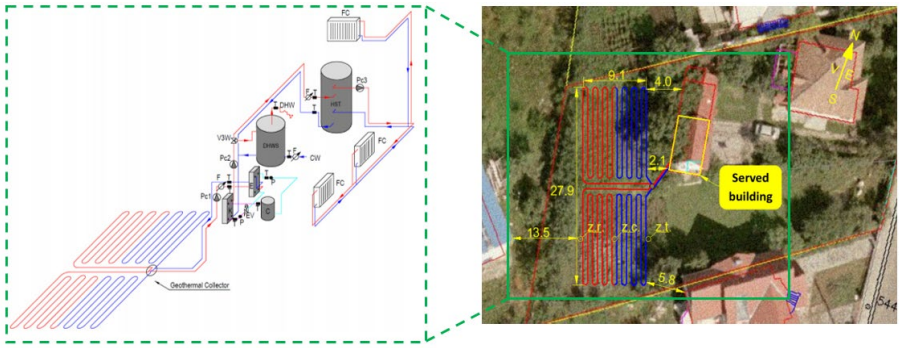

Fig. 15. The schematic diagram of GHP system applied for a small residential house [34]

Table 3 Heat transfer equations within the GHP system [34]

Description	Equation
The heat output from heat pump condenser:	$Q_k = m_w \cdot c_w \cdot \Delta t_w$
The heat source provided for heat pump evaporator:	$Q_0 = m_a \cdot c_a \cdot \Delta t_a$
The electricity consumption from heat pump compressor:	$P_C = Q_k - Q_0$
The heat pump COP:	$COP = \frac{Q_k}{P_C} = \frac{Q_k}{Q_k - Q_0}$
The whole system COP:	$COP_{SYS} = \frac{Q_k}{P_{SYS}} = \frac{Q_k}{P_C + P_w + P_a}$

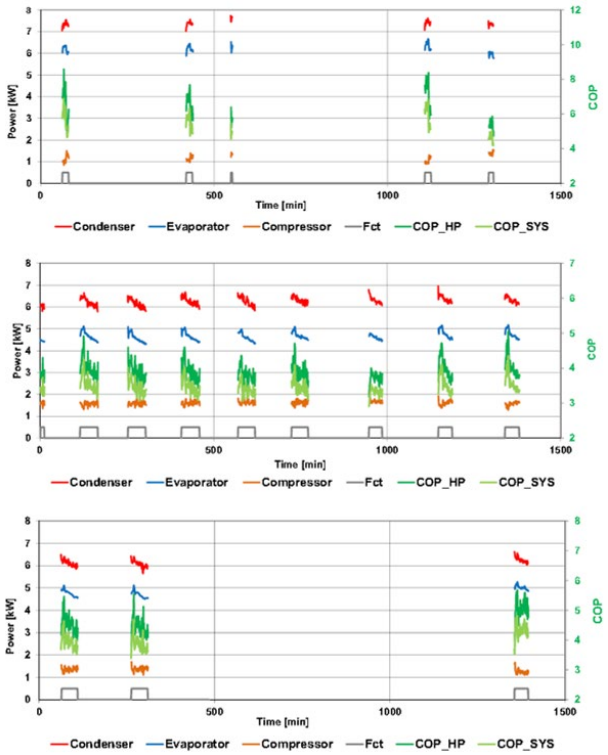

Fig. 16. Power variations of the heat pump elements, COP_{HP} and COP_{SYS}: (a) autumn; (b) winter; (c) spring [34]

Fig. 16 illustrates electricity consumption variations of the heat pump components, COP_{HP} and COP_{SYS}. The mean COP_{HP} for each operational period are 6.4 in autumn, 3.9 in winter as well as 4.7 in spring, meanwhile the mean COP_{SYS} for each operational period are 5.4 in autumn, 3.5 in winter as well as 4.0 in spring.

Sofyan et al. [35] developed an innovative three-dimensional transient model for the horizontal linear GHE with considering the impact of seasonal ground temperature change. Fig. 17 displays a graphic of the horizontal linear GHE and experimental rig.

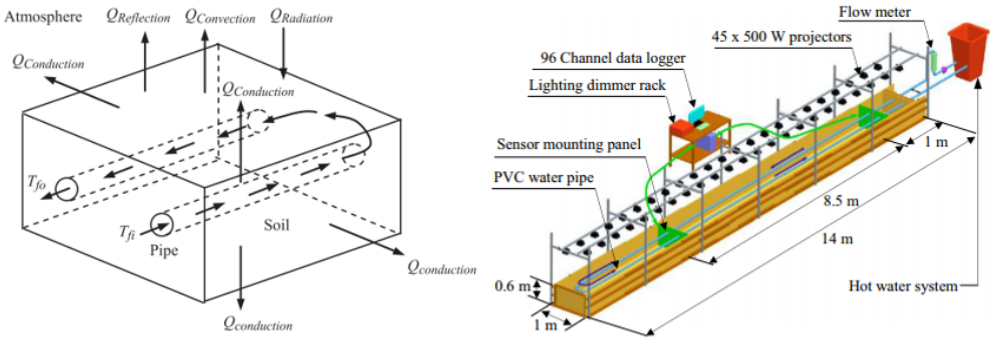

Fig. 17. Diagram of the horizontal linear GHE: (a) 3D model; (b) experimental rig [35]

The heat transfer numerical formulations in terms of the ground, pipe wall and thermal fluid are obtained as:

The ground region is given as:

$$\frac{1}{\alpha_s}\frac{\partial T_s}{\partial t}=\frac{\partial^2 T_s}{\partial x^2}+\frac{\partial^2 T_s}{\partial y^2}+\frac{H_s}{k_s} \tag{5}$$

where α_s is the soil diffusivity (m^2 /s); T_s is the soil temperature (K); t is the time period (s); H_s is the soil source term (W/m^3); k_s is the soil conductivity (W/m K); x and y are the distance in the x and y directions (m).

The pipe wall region is written as:

$$c_p\rho_p V_p\frac{\partial T_p}{\partial t}=Ah_f(T_f-T_p)+\frac{k_s A}{0.5\Delta x}(T_s-T_p) \tag{6}$$

The thermal fluid region is expressed as:

$$c_f\rho_f A\frac{\partial T_f}{\partial t}=\pi d_{in}h_f(T_p-T_f)-m_f c_f\frac{\partial T_f}{\partial z} \tag{7}$$

Fig. 18 demonstrates the calculating region of the horizontal linear GHE through the explicit finite different method (FDM), the pipe of the horizontal GHE is set as the symmetric boundary.

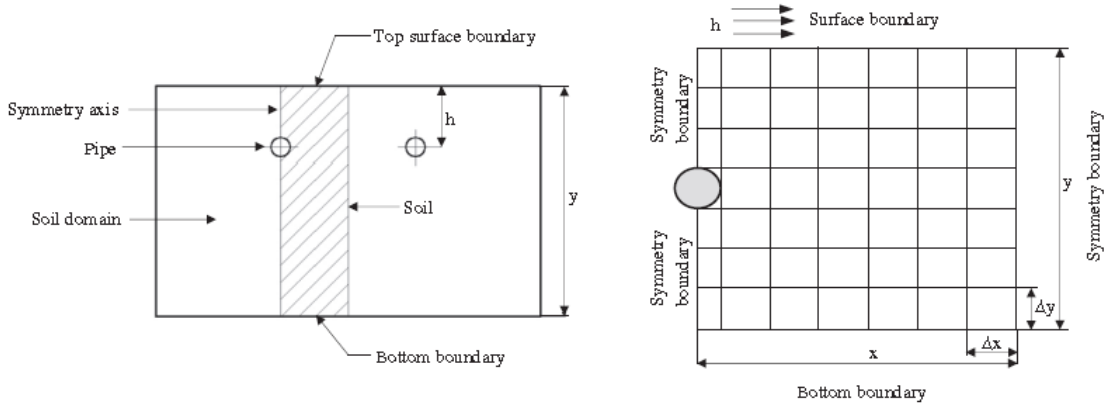

Fig. 18. Horizontal linear GHEs: (a) buried in the ground region; (b) calculating region [35]

The ground region is discretised on the basis of the structured rectangular mesh which has an equal distance in the x and y directions. The heat transfer of ground surface is affected by vegetation cover, solar radiation, evaporation and precipitation. It is found that the numerical results exhibit good precision compared with the measurement data, and the model can be used to examine the system performance and soil temperature change for a long-term operating period.

Kayaci and Demir [36] built a two-dimensional numerical heat transfer model for the horizontal GHE to simulate the system energy output for a 200 m^2 office in Istanbul. Fig. 19 depicts the soil domains and horizontal GHE pipe.

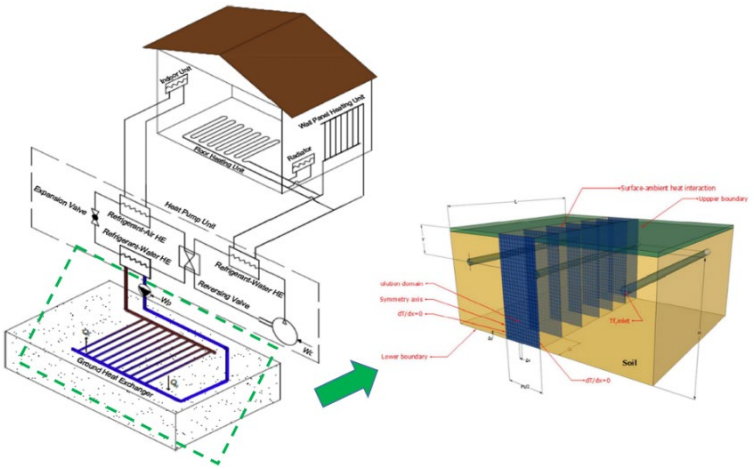

Fig. 19. Schematic of horizontal GHE pipe and soil domains [36]

The transient two-dimensional heat conduction equation is expressed as:

$$\frac{\partial^2 T}{\partial x^2}+\frac{\partial^2 T}{\partial y^2}=\frac{1}{\alpha_s}\frac{\partial T}{\partial t} \tag{8}$$

The working fluid temperature in the pipe is given as:

$$\frac{dT_{f,oi}}{dl}=\frac{q}{m_f C_{pf}}dl \tag{9}$$

where m_f is the mass fluid flow rate (kg/s); q is the heat flux (W/m^2); $C_{p,f}$ is the specific heat of fluid (J/kg·K).

Based on the energy equilibrium, the surface heat fluxes are determined with consideration of the surface-ambient heat interaction as given in Table 4. The heat transfer formulations are solved numerically by using the ADI approach which deals with the tri-diagonal matrix systems easily.

Table 4 The heat fluxes on soil surface [36]

Item	Equation
Energy equilibrium (soil surface)	$\dot{q}_t = \dot{q}_h + \dot{q}_e + \dot{q}_{ir} + \dot{q}_{er} + \dot{q}_s$
Convection	$\dot{q}_h = \rho_a C_{p,a} D_h \zeta (T_a - T_y)$; $D_h = \frac{\kappa^2 U_z}{[\ln(z/z_0)]^2}$; $\zeta = \frac{1}{(1+10Ri)}$; $R_i = \frac{gz(T_a - T_y)}{T_a U_z^2}$
Evaporation	$\dot{q}_e = 0.0168 f h_a [P_s - P_a]$
Incident radiation	$\dot{q}_{ir} = 1.08\{1 - \exp[-(0.01 e_a)^{\frac{T_a}{2016}}]\}\sigma T_a^4$
Emitted radiation	$\dot{q}_{er} = -\varepsilon\sigma T_y^4$
Solar radiation	$\dot{q}_s = (1 - \text{Albedo})[S_m + S_a \, \text{Re}(\exp(i\omega t + \varphi_1)]$

3.1.2 Slinky-coil GHE models

In comparison to the linear-loop GHE, the slinky-coil GHE uses superimposed loops arranged horizontally along the bottom of a wide trench. Based on the heat pump's specification, environmental conditions and soil properties, the slinky-coil trenches are installed from 1/3 to 2/3 shorter than conventional one. In fact, they are more space-efficient and cost-effective, and fitted in regions with restrictions on land space. Therefore, many analytical and numerical models have been established to evaluate the energy efficiency of the slinky-coil horizontal GHE.

Xiong et al. [26] established an analytical model on the basis of the principle of superposition to determine the temperature response function for the slinky-coil horizontal GHE as shown in Figs. 20 and 21.

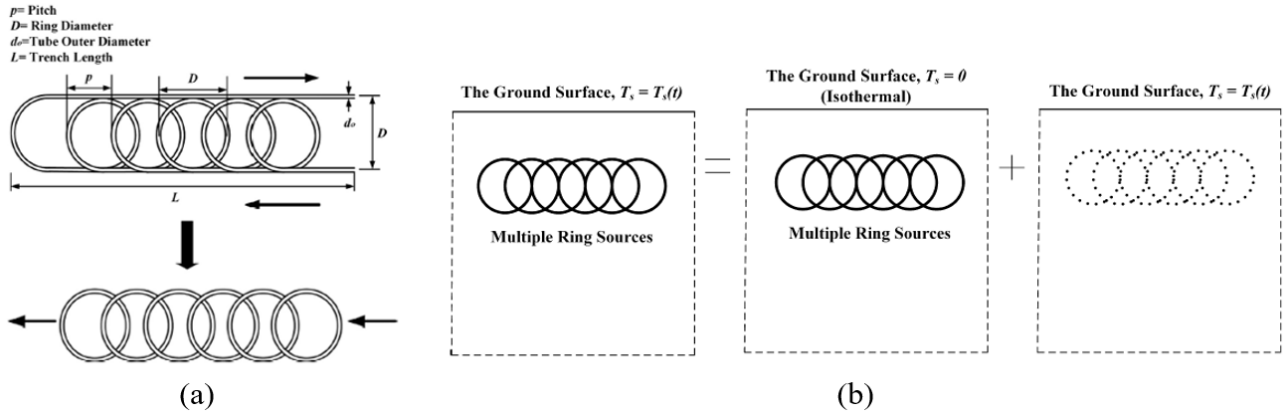

Fig. 20. (a) Simplification of a slinky loop; (b) principle of superposition [26]

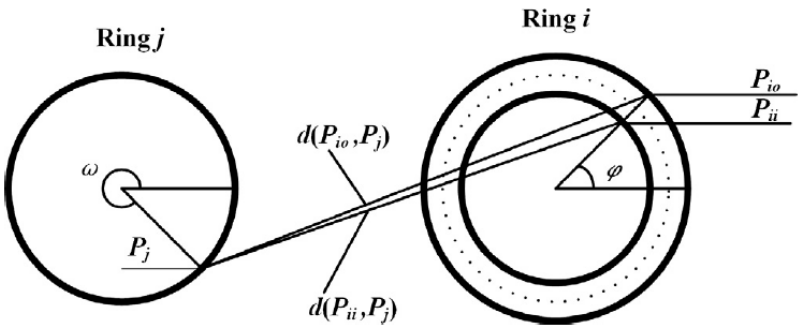

Fig. 21. Distance between points P_i and P_j on ring source j [26]

The continuous point source method is expressed as:

$$\Delta T(d,t)=\frac{q}{4\pi kd}\operatorname{erfc}\left(\frac{d}{\sqrt{4\alpha t}}\right) \tag{10}$$

where q is the heat rate (W); d is the distance between two points (m); t is the time (s); T is the temperature (°C).

The temperature perturbation at point P_i is calculated by:

$$\Delta T(P_i,t)=\frac{q_l R}{4\pi kd}\int_0^{2\pi}\frac{\operatorname{erfc}\left[\frac{d(P_j,P_i)}{2\sqrt{\alpha t}}\right]}{d(P_j,P_i)}d\omega \tag{11}$$

where P is the point; R is the radius of ring (m); i and j are the arbitrary indices.

Their simulation results indicate that ±1% deviation in temperature response factor causes the maximum ±0.2 °C error in the predicted heat pump inlet working fluid temperature for one year operating period. Meanwhile, this analytical model exhibits good precision and decreases the calculation time dramatically, making the calculation time of temperature response factor in a rational range for the whole building energy analysis.

Sangi and Müller [37] developed a called Modelica-model for the slinky-coil horizontal GHE as given in Fig. 22. The heat transfer model between the working fluid and pipe wall is developed by the Modelica Standard Library (MSL).

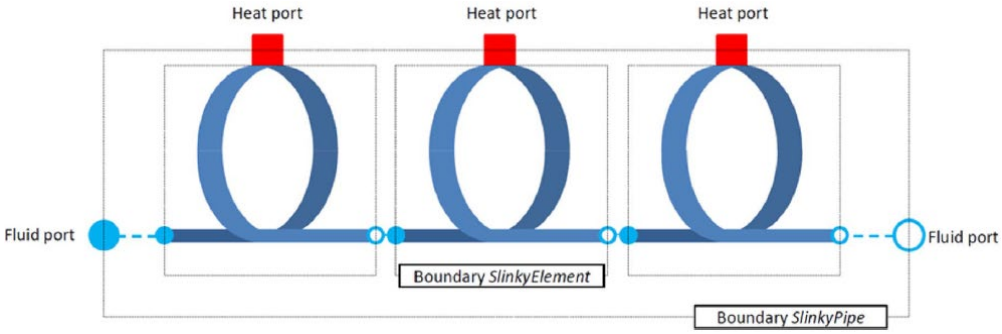

Fig. 22. Modelica-model [37]

The heat transfer equation of soil region is obtained as:

$$Q_{cond}=\lambda A\frac{T_1-T_2}{\delta} \tag{12}$$

where T_1 and T_2 are the temperatures on both sides of the wall (°C); δ is the wall thickness (m); λ is the soil thermal conductivity; A is the area (m^2).

The heat transfer between pipe wall and working fluid is written as:

$$Q_{conv} = \alpha A(T_{fluid} - T_{wall}) \tag{13}$$

where α is the heat transfer coefficient;

The radial heat transfer from the refrigerant to the external pipe wall is given as:

$$Q = \frac{2\pi L}{\frac{1}{\lambda r_{inner}} + \frac{1}{\lambda_{pipe} \times \ln(\frac{r_{outer}}{r_{inner}})}} \times (T_{fluid} - T_{wall}) \tag{14}$$

where L, r_{inner} and r_{outer} are the pipe length, internal and external pipe radii (m), respectively.

The numerical predictions are verified by the published test results, which proves the accuracy and reliability of the model.

Li et al. [38] proposed a moving ring source model considering the influence of subsoil water flow to study the temperature response of the horizontal slinky-coil GHE and multiple's performance. Fig. 23 describes the schematic diagram of a single moving ring source model within an infinite medium. In order to further simplify the calculation process, both the adiabatic and constant boundary conditions are assumed via the method of images as shown in Fig. 24.

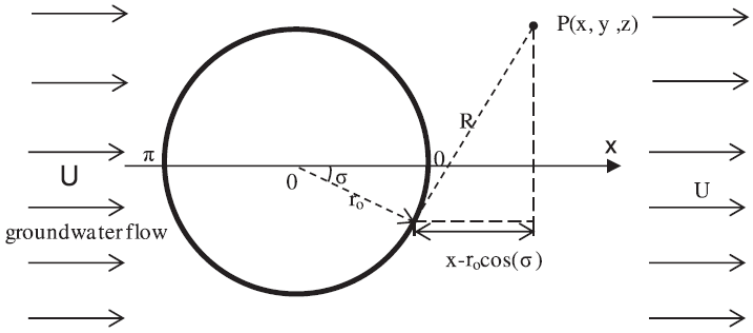

Fig. 23. Diagram of the single moving ring source method [38]

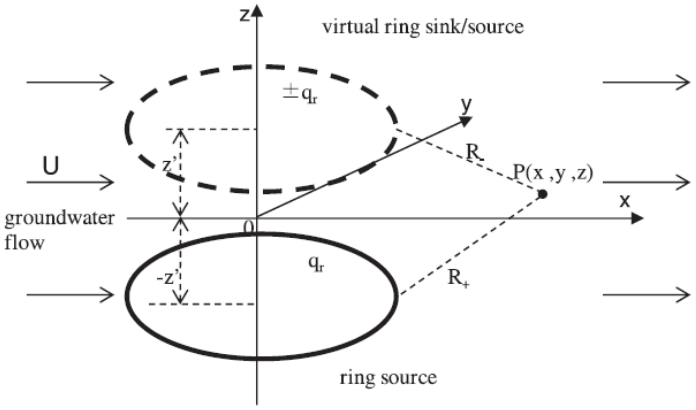

Fig. 24. The established boundary conditions by using the method of images [38]

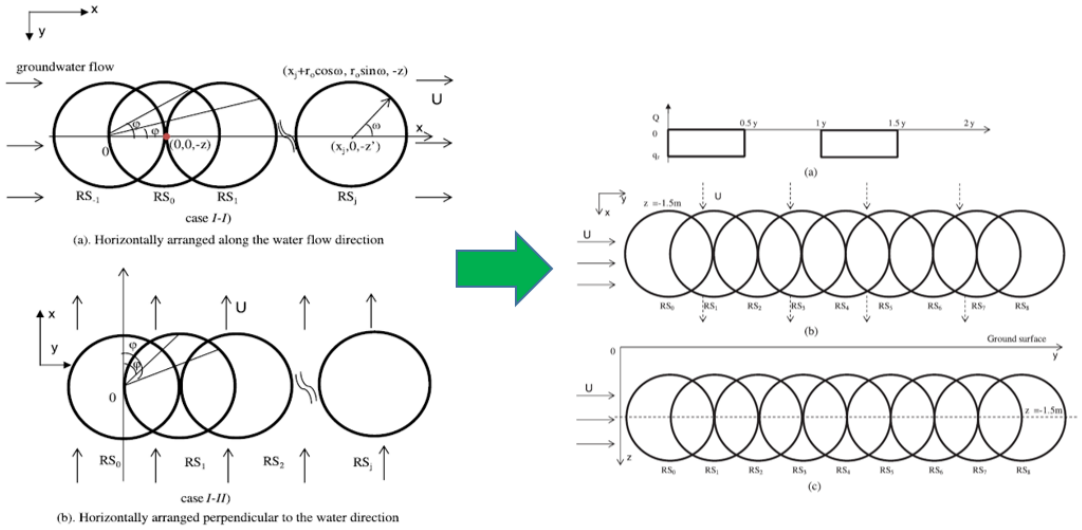

Fig. 25. Arrangements of the multiple ring sources [38]

Temperature rise at point P is given as:

$$\Theta_{inf,P}=\frac{kr_0}{q_r}\sum_{i=0}^{n-1}\Theta_{inf,i}(R_i^{'},Pe,F_0) \tag{15}$$

$$\Theta_{inf,P}=\theta_{inf}\frac{kr_0}{q_r}=\frac{1}{8}\int_0^{2\pi}\exp\{[Pe\frac{(x-\cos\sigma)}{2}]\cdot f(R_i^{'},Pe,F_0)\}d\sigma \tag{16}$$

$$f(R_i^{'},Pe,F_0)=\frac{1}{R^{'}}[\exp(-\frac{PeR^{'}}{2})erfc(\frac{R^{'}-PeF_0}{2\sqrt{F_0}})+\exp(\frac{PeR^{'}}{2})erfc(\frac{R^{'}+PeF_0}{2\sqrt{F_0}})] \tag{17}$$

where U is the groundwater constant velocity along x-direction, $Pe=\frac{Ur_0}{\alpha}$, $F_0=\frac{at}{r_0^2}$, $R^{'}=\frac{R}{r_0}$, $Z=\frac{z}{r_0}$ and $X=\frac{x}{r_0}$.

Fig. 25 illustrates the calculation process of multiple slinky ring source based on the superposition principle. When a slinky GHE comprises of n ring source units, the temperature increases at point P within a semi-infinite medium are given as:

$$\theta_{sf,P}=\frac{kr_0}{q_r^{'}}\sum_{i=0}^{n-1}\Theta_{inf,i}(R_i^{'},Pe,F_0) \tag{18}$$

$$\Theta_{sf}(R^{'},Pe,F_0)=\theta_{sf}\frac{kr_0}{q_r}=\frac{1}{8}\exp(Pe\frac{X}{2})\int_0^{2\pi}[f(R_+^{'},Pe,F_0)\pm f(R_-^{'},Pe,F_0)]d\sigma \tag{19}$$

$$R_+^{'}=\frac{(\sqrt{(x-x')^2+(y-r_0\cos\sigma)^2+[z-(-z'+r_0\sin\sigma)]^2}}{r_0} \tag{20}$$

$$R_-^{'}=\frac{(\sqrt{(x-x')^2+(y-r_0\cos\sigma)^2+[z-(z'+r_0\sin\sigma)]^2}}{r_0} \tag{21}$$

where R is the distance from point to ring source (m); F_o is the Fourier number; θ is the temperature response (°C); r is the radial coordinate (m); r_o is the ring source radius (m).

The ring coil surface temperature is written as:

$$\Theta_{sf-i} = \Theta_{sf-sur} + \sum_{j=1, j\neq i}^{n} \Theta_{sf-RS_{ij}} \tag{22}$$

where $\Theta_{sf\text{-}RSij}$ is the temperature interference from adjacent ring sources RS_j (j = 1,2,3, ……, j – i) to ring source RS_i.

$$\Theta_{sf-RS_{j0}} = \frac{1}{2\pi}\int_0^{2\pi} \Theta_{sf} d\omega \tag{23}$$

This proposed analytical model is used to study thermal efficiency of a spiral heat exchanger under different circumstances and quickly estimate the mean pipe wall temperature.

3.1.3 Spiral-coil GHE models

The horizontal spiral-coil GHE is widely utilized because it has large heat exchange area and better flow mode without air chocking in the pipes compared with the linear and slinky-coil GHEs. Moreover, the spiral-coil GHE could reduce the complication of the pipe connections and the effect of thermal short-circuiting between inlet and outlet pipes. Thereby, a number of models have been proposed in order to study thermal physical characteristics of the spiral-coil GHE.

Jeon et al. [13] developed a novel Green's function analytical model of horizontal spiral-coil GHE by the mirror image and superposition approaches. This model is used to study the influence of a semi-infinite medium and soil temperature distribution. Fig. 26 (a) shows the graphic vision of a spiral coil source for the horizontal GHE.

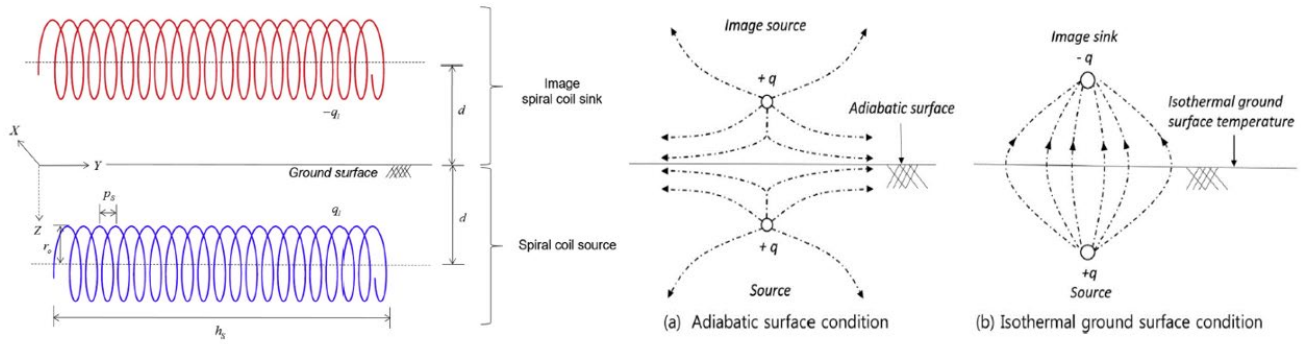

Fig. 26. (a) Horizontal spiral-coil GHE; (b) mirror image method [13]

According to Fig. 26 (b), the boundary of soil surface is regarded as isothermal or adiabatic condition, relying on the symbol of the source in the image. The temperature change because of the image spiral-coil GHE is given as:

$$\theta(u,t) = \frac{q_l}{\rho c}\int_0^t\int_0^\infty G(u,t|u',t)du'd\tau = \frac{q_l}{8(\pi\alpha)^{3/2}}\int_0^t \frac{1}{(t-\tau)^{3/2}}\int_0^{h_s} e^{-\frac{F_{im}(x,y',z)+(y-y')^2}{4\alpha(t-\tau)}} dy'd\tau \tag{24}$$

$$F_{im}(x,y',z) = x^2 + (z+d)^2 + r_0^2 - 2xr_0\cos(\frac{2\pi y'}{ps}) - 2(z+d)r_0\sin(\frac{2\pi y'}{ps}) \tag{25}$$

$$\theta(u,t)=\frac{q_l}{\rho c}\int_0^t\int_0^\infty G(u,t|u',t)du'd\tau=\frac{q_l}{8(\pi\alpha)^{3/2}}\int_0^t\frac{1}{(t-\tau)^{3/2}}\int_0^{h_s}e^{-\frac{F_0(x,y',z)+(y-y')^2}{4\alpha(t-\tau)}}-e^{-\frac{F_{im}(x,y',z)+(y-y')^2}{4\alpha(t-\tau)}}dy'd\tau \quad (26)$$

$$F_0(x,y',z)=x^2+(z-d)^2+r_0^2-2xr_0\cos(\frac{2\pi y'}{ps})-2(z-d)r_0\sin(\frac{2\pi y'}{ps}) \quad (27)$$

where u' is the position of the image spiral coil source; q is the temperature (°C); Q (u, t) is the source density; u is the position vector.

The error equation is written as:

$$\theta(u,t)=\frac{q_l}{4\pi\lambda}\int_0^h\frac{\mathrm{erfc}[A_0(u,y')/2\sqrt{\alpha t}]}{A_0(u,y')}-\frac{\mathrm{erfc}[A_{im}(u,y')/2\sqrt{\alpha t}]}{A_{im}(u,y')}dy' \quad (28)$$

$$A_{0/im}(u,y')=\sqrt{F_{0/im}(x,y',z)+(y-y')^2} \quad (29)$$

The results of the numerical model display a good fit with the experiment data with an average difference of 0.3%. The model is capable of capturing the structure of the spiral coil accurately, and therefore it provides a more precise assessment for the soil temperature.

Kim et al. [29] established a 3D numerical model of HGHE by CFD software as presented in Fig. 27. The 3D numerical model has 472626 elements that are setup as a tetrahedral type. The average mesh element quality is about 0.6581. It can be obtained from Fig. 28 that the outlet fluid temperature is lower than the inlet fluid temperature, finally reaches 32.09 °C which is lower than the entering water temperature of 32.2 °C.

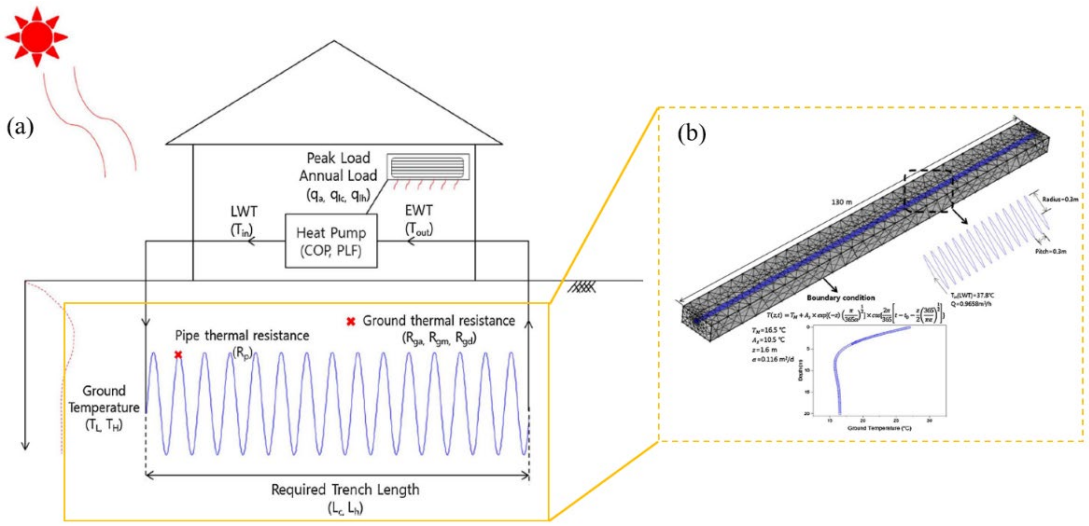

Fig. 27. (a) Horizontal spiral-coil GHE; (b) CFD model and boundary conditions [29]

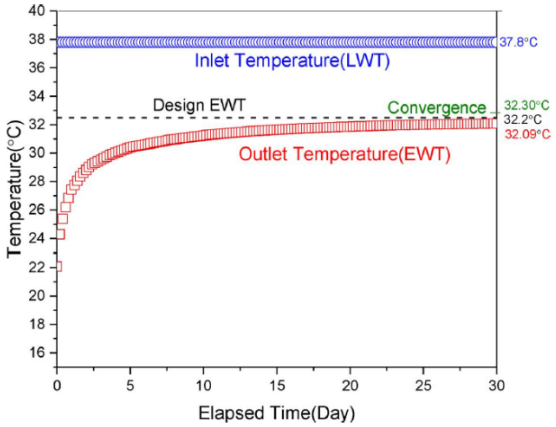

Fig. 28. Numerical simulation results [29]

Li et al. [39] studied the operating features of the horizontal spiral-coil GHP to analyse the influences of heat pump and groundwater movement on the system performance as illustrated in Fig. 29.

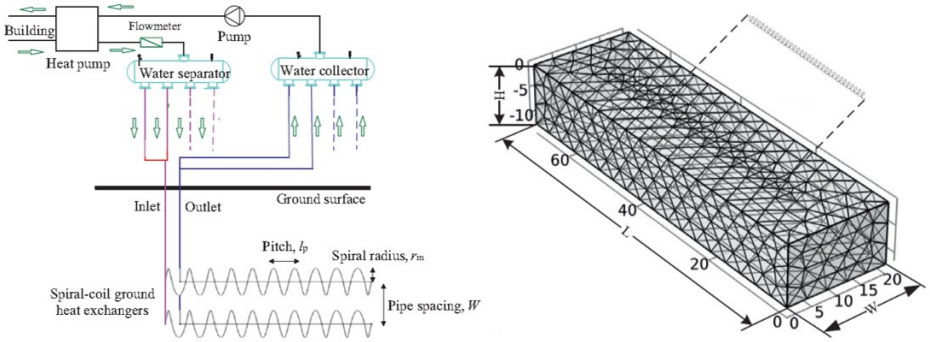

Fig. 29. The schematic of the horizontal spiral-coil GHP system [39]

The heat transfer model between the working fluid and pipe is illustrated as [39]:

$$\rho_f A_p C_{p,f} \frac{\partial T_f}{\partial t} + \rho_f A_p C_{p,f} u \cdot \nabla T_f = \nabla \cdot (A_p k_f \nabla T_f) + \frac{1}{2} f_D \frac{\rho_f A_p}{d_h} |u| u^2 + Q_{Wall} \quad (30)$$

A_p is the cross section area of pipe (m^2); q_f is the working fluid density (kg/m^3); t is the time (s); u is the working fluid velocity (m/s); f_D is the Darcy friction factor; dh is the hydraulic pipe diameter (m); T_f is the working fluid temperature (°C); $C_{p,f}$ is the heat capacity of fluid (J/kg·°C); k_f is the thermal conductivity of fluid (W/m·°C).

The heat transfer between the ground and pipe is given as [39]:

$$Q_{wall} = (hZ)_{eff} (T_s - T_f) \quad (31)$$

where T_s is the ground temperature (°C); $(hZ)_{eff}$ is the whole thermal resistance of the pipe wall (K/W).

The thermal resistance in a circular pipe is written as:

$$(hZ)_{eff} = \frac{2\pi}{\frac{1}{r_i h_i} + \frac{\ln(\frac{r_o}{r_i})}{k_p}} \quad (32)$$

where r_i and r_o are the inner and outer radius of the pipe respectively (m); h_i is the convection coefficient within the pipe ($W/m^2 \cdot °C$); k_p is the thermal conductivity of the pipe wall ($W/m \cdot K$).

The heat exchange within the soil region is described as:

$$\rho_s C_{p,s} \frac{\partial T_s}{\partial t} = \nabla \cdot (k_s \nabla T_s) - Q_{wall} \tag{33}$$

where subscript s denotes the soil.

In heating season, the thermal load of GHE (Q_{GHE}) is given as:

$$Q_{GHE}^{heating} = Q_{building}(1 - \frac{1}{COP_{heating}}) \tag{34}$$

In cooling season, the thermal load of GHE (Q_{GHE}) is expressed as:

$$Q_{GHE}^{cooling} = Q_{building}(1 + \frac{1}{COP_{cooling}}) \tag{35}$$

Electricity input to the compressor of heat pump is calculated by:

$$P = \frac{Q_{GHE}}{COP} \tag{36}$$

where P is the heat pump power (W); COP is the coefficient of performance; Q_{GHE} is the thermal load of GHE (W).

The initial and boundary conditions are given in Table 5.

Table 5 The initial and boundary conditions [39]

Description		Equation
Initial conditions	The initial conditions of the soil and fluid are regarded as same	$T_{s/f}(x,y,z,t)\big\|_{t=0} = T_s(z,t)\big\|_{t=0}$
	The soil temperature T_s (z,t)	$T_s(z,t) = T_{mean} - T_{amp} e^{-z\sqrt{\frac{\omega}{2\alpha_s}}} \cos[\omega(t - tc) - z\sqrt{\frac{\omega}{2\alpha_s}}]$
Boundary conditions	At wall z = 0	$T_s(x,y,z,\tau)\big\|_{z=0} = T_{mean} - T_{amp} \cos[\omega(t - t_c)]$
	At wall z = H	$T_s(x,y,z,\tau)\big\|_{z=H} = T_S(z,\tau)\big\|_{z=H}$
	At wall y = 0 and y = L	$T_s(x,y,z,\tau)\big\|_{y=0,y=L} = T_s(z,\tau)\big\|_{y=0,y=L}$
	At wall x = 0 and x =W	$\frac{\partial T_s(x,y,z,t)}{\partial x}\Big\|_{x=0,x=W} = 0$

Fig. 30 illustrates the comparison among outlet fluid temperatures calculated by numerical model and Mei's model, and experiment data. It can be found that the outlet fluid temperatures in numerical model give a good agreement with the test results. The maximum and average errors are 1.1 °C and 0.2 °C, respectively [39].

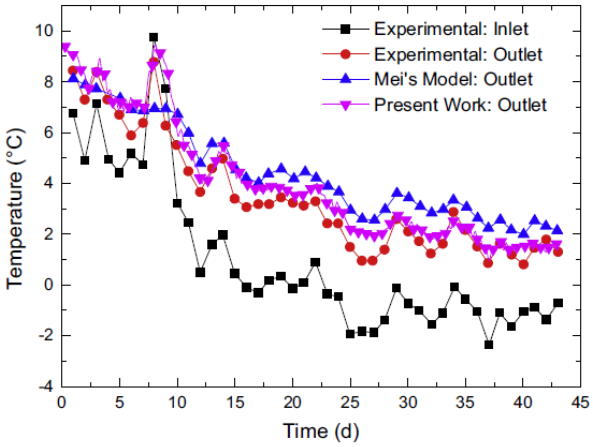

Fig. 30. Comparison among numerical model, experimental results and Mei's model [39]

Moreover, the results reveal that the differences between mean inlet fluid temperatures with and without heat pump in cooling and heating modes reach 4.1% and 11.5%, respectively. Furthermore, the pipe spacing and soil thermal conductivity have great influences on the horizontal GHP system performance.

Kim et al. [40] simulated a horizontal spiral-coil GHE to compare its heat transfer rate with the slinky-coil GHE's by using the computational fluid dynamics (CFD) software as shown in Fig. 31.

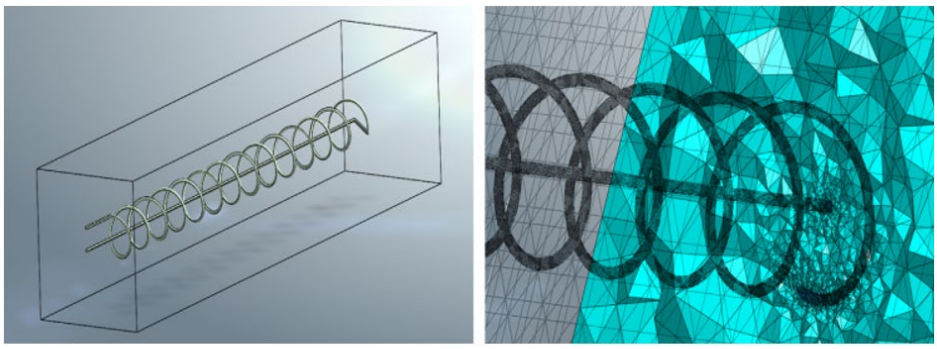

(a) (b)

Fig. 31. Numerical simulation: (a) 3D geometric model; (b) mesh model [40]

Small error of about 8–10% between the numerical and experimental results is obtained. It is concluded that the horizontal spiral-type GHP could achieve better performance than the slinky-coil GHP. In addition, the soil thermal conductivity and GHE configurations are the key factors to calculate the GHE heat transfer rate while the pipe diameter has little impact on the GHE performance.

Go et al. [31, 41] established a three-dimensional model of a horizontal spiral-coil loop to investigate thermal behaviour based on the FEM as shown in Fig. 32 (a).

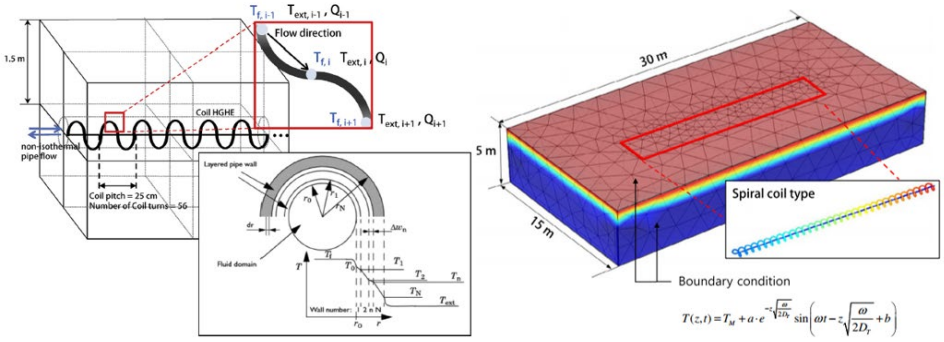

(a) (b)

Fig. 32. (a) Heat transfer process; (b) finite element model [31, 41]

The heat transfer equation in the region is expressed as:

$$(\rho C)u\left(\frac{\partial T}{\partial x}+\frac{\partial T}{\partial y}+\frac{\partial T}{\partial z}\right)-\lambda\left(\frac{\partial^2 T}{\partial x^2}+\frac{\partial^2 T}{\partial y^2}+\frac{\partial^2 T}{\partial z^2}\right)=Q \tag{37}$$

where u is the fluid velocity (m/s); T is the soil temperature (°C); λ is the soil thermal conductivity (W/m·K); Q is the heat sources (W/m^3).

The fluid equation within a pipe is given as:

$$\rho_f A_p C_p \frac{\partial T_f}{\partial t}+\rho_f A_p C_p u\cdot\nabla T_f=\nabla\cdot(\lambda A_p \nabla T_f)+\frac{1}{2}f_D\frac{\rho A_p}{2d_h}|u|u^2+Q+Q_{wall} \tag{38}$$

where r_f is the refrigerant density (kg/m^3); A_p is the area of pipe cross-section (m^2); C_p is the specific heat capacity at a constant pressure (J/kg·°C); u is the fluid velocity (m/s); $1/2f_D\rho A_p/2d_h$ is the friction heat dissipated due to viscosity; Q is the normal heat source (W/m); Q_{wall} is the heat source term (W/m).

The heat transfer equation between the working fluid and solid mass is written as:

$$Q_{wall}=(hZ)_{eff}(T_{ext}-T_f) \tag{39}$$

where T_{ext} is the external temperature outside the pipe (°C); Z is the perimeter of the pipe wall (m).

To analyse heat exchange of the horizontal GHE, a finite element model is established with dimensions of 30 m× 15m × 5 m by COMSOL Multiphysics software as depicted in Fig. 32(b).

According to Fig. 33, the mean relative error is less than 2.5% between the prediction of the numerical model and test data. It is concluded that the rainfall infiltration leads to a widening working fluid temperature gap between the inlet and outlet, and it could increase the thermal efficiency. Meanwhile, the groundwater movement has a positive influence on the system performance, and the advection effect varies with the soil hydraulic conductivity and void ratio.

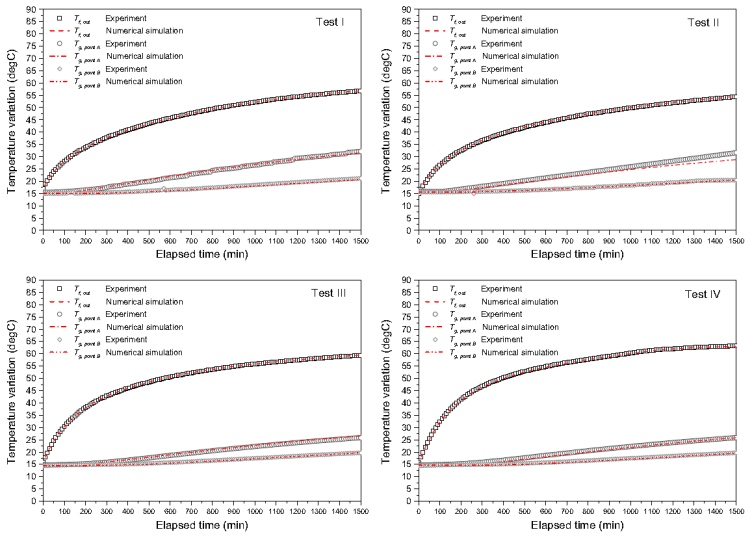

Fig. 33. Validation between numerical and experimental results [41]

3.1.4 Comparison of technical models

To decrease the horizontal GHE pipe length, required land region and enhance thermal performance, the comparative study of analytical and numerical models is done for three types of the horizontal GHE .

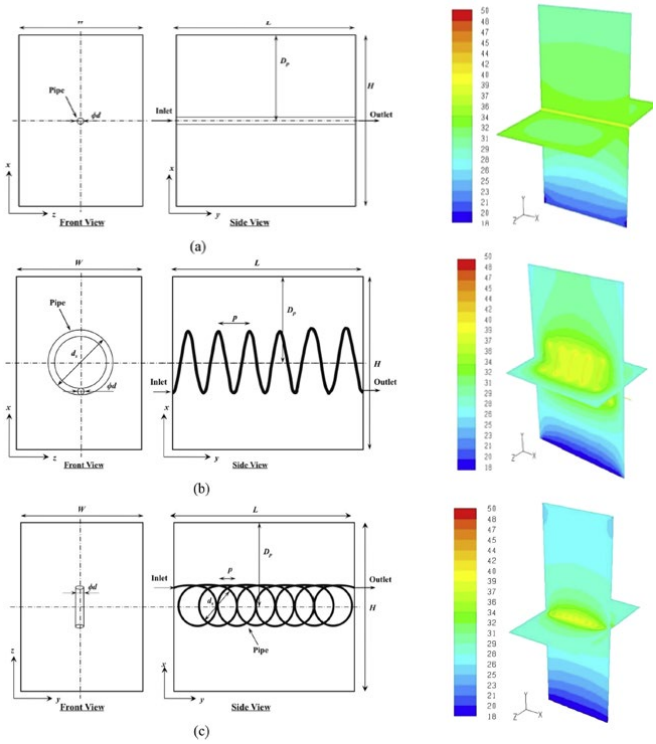

Fig. 34. Diagram of a horizontal GHEs (a) linear; (b) helical; (c) slinky [15]

Dasare and Saha [15] analysed the annual performance of the horizontal GHE with different configurations based on three-dimensional FEM model for short-term operation as presented in Fig. 34. It is revealed that the spiral coil-type GHE presents superior performance in the light of heat energy extraction compared with the linear horizontal GHE. Moreover, the trench depth is not a significant factor affecting the GHE performance.

Habibi and Hakkaki-Fard [42] presented a three-dimensional numerical model by the finite volume method (FVM) to evaluate thermal performances of different horizontal GHEs as given in Fig. 35. The diagram of the heat transfer analysis based on the equivalent thermal resistance circuit is given in Fig. 36.

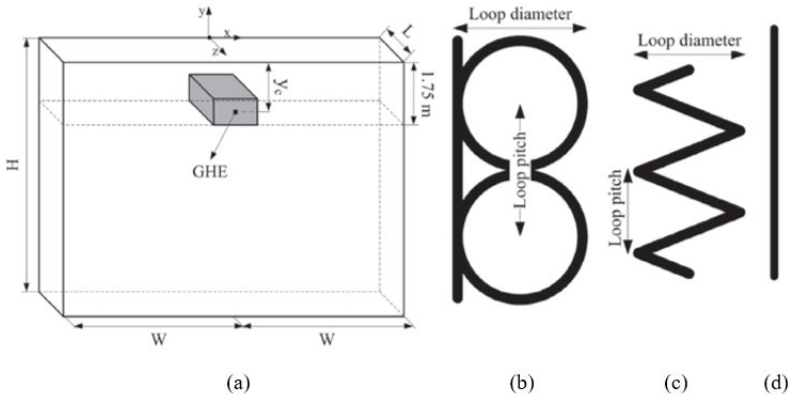

Fig. 35. Schematic diagram of GHEs (a) calculation domain; (b) slinky; (c) spiral; (d) linear [42]

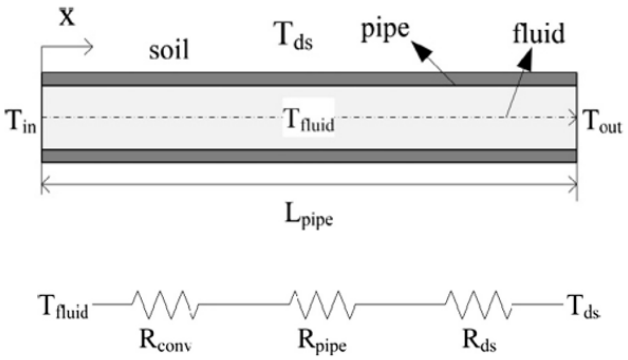

Fig. 36. The heat transfer analysis based on the thermal resistance circuit [42]

The heat transfer rate along the buried GHE pipe is obtained as:

$$dQ = (T_{ds} - T)(\frac{1}{R_{GHE}})dx \tag{40}$$

where T is the circulating fluid temperature (°C); T_{ds} is the soil temperature nearby the pipe (°C); R_{GHE} is the GHE thermal resistance (W/m).

The disturbed soil temperature is given as:

$$T_{ds}(t) = T_{soil}(y,t)\big|_{y=y_c} + f(t) \tag{41}$$

where y_c is the depth of the GHE center (m); f(t) is the thermal influence of the GHE on the soil surrounding the pipe (m).

The overall heat transfer rate is expressed as:

$$dQ = m_{water} C_{water} \frac{dT}{dx} dx \tag{42}$$

where m_{water} is the water mass flow rate (kg/s); C_{water} is the specific heat of water (kJ/kg·s).

The thermal load of the GHE is given as:

$$Q_{GHE} = Q_{building}(1 - \frac{1}{COP}) \quad (43)$$

$$COP = \frac{Q_H}{Q_H - Q_L} \quad (44)$$

$$Q_{building} = \frac{3}{4}A_0 \sin[\frac{2\pi}{8760}(t - t_0) + \frac{1}{4}\left|A_0 \sin[\frac{2\pi}{8760}(t - t_0)]\right| \quad (45)$$

where Q_H is the heat transfer rate in the heat pump condenser such as the building thermal demand ($Q_{building}$) (kW); Q_L is the heat transfer rate in the heat pump evaporator such as the GHEs load (Q_{GHE}) (kW); A_0 is the maximum amount of heat that is injected to the building by the GHP during the cold period of the year (kW). The thermal resistance equations within the GHE are illustrated in Table 6. The results indicate that the linear arrangement has the highest heat transfer rate per pipe length.

Table 6 The thermal resistance heat transfer equations within the GHE [42]

Description	Equation
The thermal resistance of GHE (R_{GHE}):	$R_{GHE} = R_{conv} + R_{pipe} + R_{ds}$
The thermal resistance between the internal pipe wall and fluid:	$R_{conv} = \frac{1}{\pi D_{in} h_c}$
The thermal resistance of the pipe wall:	$R_{pipe} = \frac{\ln \frac{D_{out}}{D_{in}}}{2\pi k_{pipe}}$
The thermal resistance between external pipe wall and soil:	$R_{ds} = \frac{1}{2\pi k_{soil}}[\ln(\frac{D_{out} + d_{constant}}{2D_{out}})]$

Furthermore, an innovative design concept for the height of the secondary soil (HSS) is proposed to improve thermal performance of the horizontal GHE system. Fig. 37 depicts the schematic of spiral GHE in parallel arrangement with secondary soil. The HSS is defined as the height of the secondary soil used on top of the GHE.

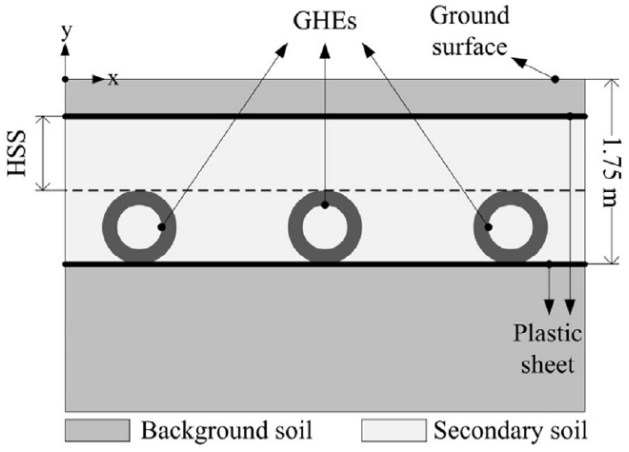

Fig. 37. Schematic diagram of horizontal GHEs buried in secondary soil [42]

According to Fig. 38, it can be concluded that the secondary soil has better heat transfer rate during 80% of the heating season. Meanwhile, it is also demonstrated that the saturated secondary soil is able to decrease the initial installation expense of the GHE up to 40% in comparison with the system without the secondary soil.

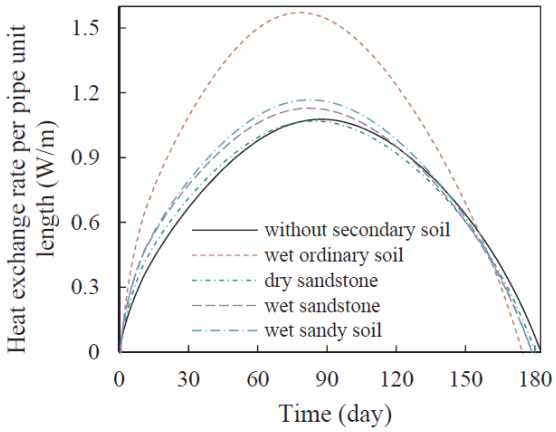

Fig. 38. Influence of different secondary soil types on heat transfer rate of horizontal GHE [42]

Han et al. [43] established a three-dimensional heat transfer model of the horizontal GHP to calculate the annual system performance for various GHE arrangements. Fig. 39 exhibits the geometries of those horizontal GHE configurations. Results of this study demonstrate that the soil temperature and thermal properties contribute to enhancing the GHE system performance for long-term and short-term operating periods.

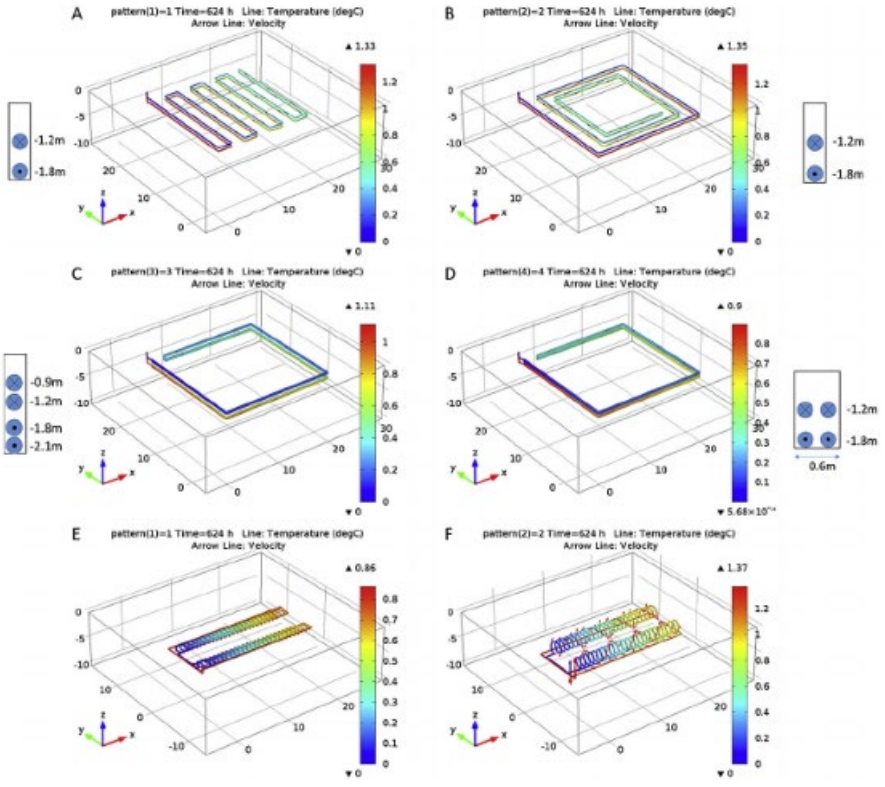

Fig. 39. Geometry of different horizontal GHEs in heating mode [43]

Selamat et al. [44] developed a three-dimensional CFD model to optimize the design for the horizontal GHE by means of different GHE arrangements and pipe materials. Fig. 40 shows the pressure distributions of flow path under different layouts. It is found that the slinky-coil GHE has high heat transfer rate compared to the straight GHE. Furthermore, copper pipe could improve energy efficiency by 16% over high-density polyethylene (HDPE) pipe.

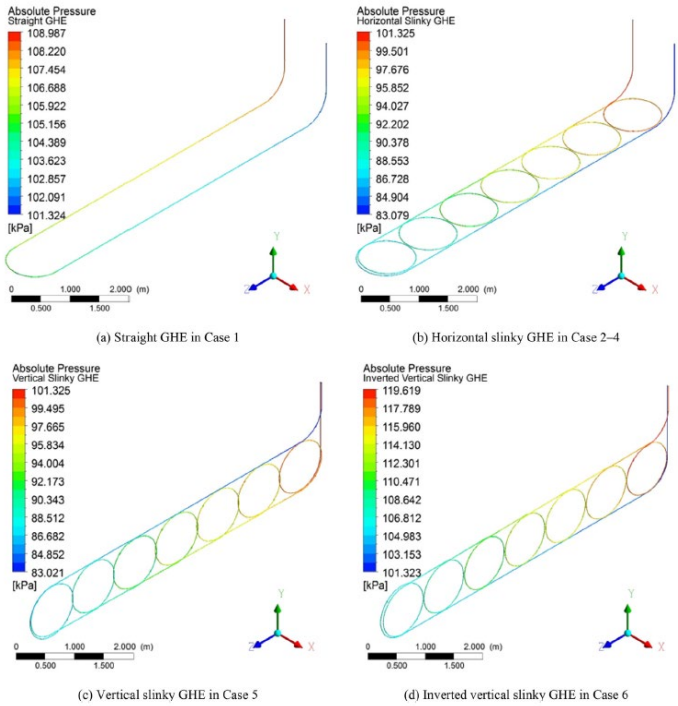

(a) Straight GHE in Case 1 (b) Horizontal slinky GHE in Case 2–4

(c) Vertical slinky GHE in Case 5 (d) Inverted vertical slinky GHE in Case 6

Fig. 40. Schematic diagram of pressure distribution: (a) linear; (b) slinky; (c) vertical slinky; (d) inverted vertical slinky [44]

To sum up, the merit of analytical models is that the straightforward complicated mathematical algorithm could be easily combined into a simulation/design program. Meanwhile, the essential calculation time of the analytical method is much less in comparison to the numerical method's. However, the accuracy of analytical results is slightly low because of the assumptions and simplifications. Therefore, the numerical models are more attractive to attain high accurate results based on the FEM, FDM, FVM, ADI and commercial software. It is found that the numerical models of the horizontal GHE normally conduce to more comprehensive investigations of the GHP performance in the design and optimization phases. In comparison to the analytical models, the numerical models often provide a better approximation of the energy efficiency, temperature variation as well as soil heat and mass transfer rates. Nevertheless, they are impractical for engineering application for three reasons as below: 1) numerical models are more time-consuming and complicated for the computing process; 2) it is very difficult to setup a normal mesh production program for different arrangements; 3) the majority of the numerical methods are performed by the CFD, Matlab, COMSOL and FEFLOW software. Table 7 demonstrates the comparison of the main analytical and numerical models for the horizontal GHE.

492 **Table 7** Comparison of analytical and numerical models

Technical models							
	Model	**Type**	**Assumption conditions**	**Initial and boundary conditions**	**Key findings**		
					Approaches used	**Error assessment**	**Scope of applications**
Analytical models	Neupauer et al. [17]	Linear-loop GHE	1) The thermal interaction is overlooked between soil surface and nearly soil; 2) The refrigerant temperature variation alongside the pipe length is ignored.	1) The initial soil temperature is set as 21.49 °C; 2) The initial heat flux is defined as 48.2W/m; 3) The soil surface is defined as: $T = T_{init} + \frac{q_s}{k}[\sqrt{\frac{4\alpha t}{\pi}}\exp(-\frac{y^2}{4\alpha t}) - y \cdot \mathrm{erfc}(\frac{y}{2\sqrt{\alpha t}})]$	Based on the line source model.	The difference between the 1D analytical model and experimental analysis is approximately 20%-30%.	To assess the long-term variation in the soil temperature.
	Xiong et al. [26]	Slinky-coil GHE	1) The heat flux is uniform along a ring; 2) The heat flux of every ring within the GHE region is the same; 3) The soil is regarded as a semi-infinite uniform medium;	1) The initial condition is defined as: $T^{1+2}(x,z,0) = T^1(x,z,0) + T^2(x,z,0)$ 2) The soil surface is set as : $(T_s - T)\alpha_s = -k\frac{dT}{dz}$ $T = T_s(t), z = 0$	Based on the principle of superposition.	The maximum error of the inlet fluid temperature of heat pump is only 0.8% between analytical model and experimental result.	1) To calculate the thermal influence of the soil temperature change; 2) To calculate the system performance and energy output; 3) To significantly improve computation speed.
	Sangi and Müller [37]	Slinky-coil GHE	1) The heat transfer of ground is assumed as the heat conduction; 2) The influence of heat radiation and convection are neglected in the model; 3) The ground temperatures at the surfaces are set to be constant.	1) The boundary of calculation domain is set as 55×24×10m; 2) The pipes of the GHE are laid out 1.5 m below the surface.	Based on the thermal resistance method.	The deviation is about 2.1 °C between the analytical model and test result.	To evaluate the system performance and parameter analysis.
	Li et al. [38]	Slinky-coil GHE	1) The soil surface is regarded as the constant value; 2) The soil is treated as a homogeneous infinite porous medium; 3) The velocity of soil groundwater flow is assumed as a constant value along one direction;	1) The average original ground temperature is defined from the ground surface to the depth of 5m; 2) The working fluid temperature of 20 °C is set as the initial temperature; 3) The adiabatic boundaries are set between the symmetry of the heat source and virtual heat sink/source.	Based on the Green's function and line source model.	The relative difference is less than 2% based on the error functions.	1) To analyze the thermal performance with considering the ground water flow; 2) To determine the pipe wall, soil temperature.
	Jeon et al. [13]	Spiral-coil GHE	1) The calculation domain is defined as a homogeneous, isotropic solid body; 2) The model is assumed in the semi-infinite medium.	1) The initial condition is given as: $\theta(u,0) = j(u,0)$; 2) The Dirichlet boundary condition is set as: $\frac{\partial\theta}{\partial t} - \alpha\Delta\theta = Q(u,t)$; $\theta(u,t) = h(u,t)$.	Based on the Green's theory and mirror image method.	The error between the analytical and experimental results is about 0.3%.	To provide a more accurate prediction of soil temperature.
	Habibi and Hakkaki-Fard [42]	Linear-loop, slinky-coil, and spiral-coil GHEs	1) System is utilized merely for space heating; 2) All components are regarded as the steady-state; 3) All thermal and physical properties of materials are set as the uniform; 4) Soil is treated as the homogeneous medium; 5) Heat transfer in the soil region is defined as pure heat conduction;	1) The initial soil temperature is defined as the undisturbed soil temperature; 2) The soil surface and bottom boundaries of the domain are defined as the undisturbed soil temperature; 3) The mean working fluid temperature is set as the inlet fluid temperature of the simulated loop.	Based on the thermal resistance method.	The maximum error observed from the experimental data is about 4.5% compared with the analytical results.	1) To investigate the thermal performance and initial installation cost among the three types of GHEs; 2) To assess the effect of the secondary soil layer on the three types of GHEs system performance.

			6) The pipe wall is assumed to be smooth with no-slip condition.				
Numerical models	Kupiec et al. [18]	Linear-loop GHE	1) The ground is treated as a semi-infinite body; 2) The soil is regarded as a heat conduction process; 3) The heat exchange between the soil and environment is assumed as heat convection.	1) The initial condition is given as: t=0: T=f(x); 2) The first boundary condition for the soil surface is x=0: $-k\frac{dT}{dx}=h_0(T_a-T_o)$ 3) The second boundary condition is given as: $x\to\infty$, $T=T_b$	Model equations are solved by the FDM using the Cranke Nicolson scheme.	The soil temperature difference in the simulated model is are consistent with the experimental results (error <10%).	1) The model can be used to determine the soil surface temperature and heat transfer rate from soil to working fluid; 2) The mean temperature of the subsurface layer of the soil are determined.
	Noorollahi et al. [33]	Linear-loop GHE	1) The greenhouse and soil are regarded as the heat sources or sinks; 2) Heat transfer model is divided into two parts, namely internal and external of the greenhouse.	1) The initial condition is written as: $\frac{\partial T}{\partial r}(0,t)=0$; 2) The boundary condition is given as: $T(r\to\infty,t)=T_g$; $T(r,0)=T_g$.	The heat transfer equation is solved by the Cranke-Nicolson method based on the Matlab software.	The maximum error is about 13.1% between numerical model and test results.	1) The proposed model can be utilized to obtain the GHP system energy output for greenhouse; 2) To Analyse the heat transfer process between soil and working fluid.
	Sofyan et al. [35]	Linear-loop GHE	1) The heat transfer in the soil domain is assumed as the pure heat conduction; 2) The heat transfer between working fluid and soil is regarded as 2D model.	1) The soil seasonal variation are determined via using an interior source term method: $H_s=\rho_s c_s\frac{\Delta T_s}{\Delta t}$; 2) The soil temperature is assumed as the constituent value at the depth of 10m; 3) The computational domain of soil is treated as the symmetry boundary.	1) The 3D model is solved based on the explicit FDM; 2) The time step Δt is given based on the Courant–Friedrichs–Lewy stability condition: $\lvert\psi\rvert\le 1, \Delta\le\frac{\Delta z}{\upsilon_f}$	1) The maximum soil temperature error between the 3D model and the measured result is 0.3 °C; 2) The measured outlet fluid temperature is higher than the 3D model.	The model is used to conduct a sensitivity analysis to investigate the effects of the pipe length, fluid flow rate and inlet working fluid temperature of the horizontal GHE.
	Kayaci and Demir [36]	Linear-loop GHE	1) The horizontal parallel pipes are assumed as the same depth; 2) The influences of mass transfer to total heat transfer rate are overlooked; 3) Ground thermal properties is regarded as the constant; 4) The working fluid rate is the same within each pipe;	1) The initial condition is given as: $T(x,t)=T_{s,m}+T_{s,a}e^{-Y\sqrt{\frac{\pi}{\alpha_s P}}}\cos(2\pi\frac{t}{P}-Y\sqrt{\frac{\pi}{\alpha_s P}})$ 2) The boundary conditions are given as: $T_i=T(x,t)$, t=0; $\left.\frac{\partial T}{\partial x}\right\rvert_{x=P_s/2}=0$; $\left.\frac{\partial T}{\partial x}\right\rvert_{x=P_s/2}=0$; q (W/m^2), y=H; q_t (W/m^2), y=0.	Based on the ADI method.	The maximum errors between numerical and experimental results of mean inlet and outlet working fluid temperatures are verified as 1.09°C and 0.86°C, respectively.	1) The model is used to solve efficiently with the tri-diagonal matrix algorithm; 2) The model can be used to determine the annual heating and cooling energy output for a long-term operation.
	Li et al. [39]	Spiral-coil GHE	1) The heat exchange between soil and working fluid is assumed as the pure heat conduction; 2) The thermal load of GHEs is assumed to be equal to the building demands; 3) COP is calculated by: $COP=0.003T_{f,0}^2+0.056T_{f,0}^2+5.784$	1) The initial conditions of the working fluid and ground are considered as the same: $T_{s/f}(x,y,z,t)\rvert_{t=0}=T_s(z,t)\rvert_{t=0}$; 2) The soil boundary condition are given as: z=0, $T_s(x,y,z,t)\rvert_{z=0}=T_{mean}-T_{amp}\cos[\omega(t-t_c)]$; 3) z=H, $T_s(x,y,z,t)\rvert_{z=H}=T_s(z,\tau)\rvert_{z=H}$; 4) y=0 and y=L, $T_s(x,y,z,t)\rvert_{y=0,y=L}=T_s(z,\tau)\rvert_{y=0,y=L}$; 5) x=0 and x=W, $\left.\frac{\partial T_s(x,y,z,t)}{\partial x}\right\rvert_{x=0,x=W}=0$	Based on the FEM.	The maximum error of outlet fluid temperature is 1.1 °C and the mean error is 0.2 °C.	1) To study the effect of heat pump COP, ground and working fluid temperatures; 2) To analyse the impact factors including the pipe spacing, buried depth as well as soil thermal conductivity, on system performance.
	Kim et al. [40]	Spiral-coil GHE	The heat transfer process is treated as the heat conduction in the ground region.	1) The initial inlet working fluid temperature is set as 16 °C; 2) The boundary of model is defined as 5m×1m×1m.	Based on the FEM and CFD.	The difference is about 8%–10% between numerical	1) To precisely assess the thermal performance of the horizontal GHEs; 2) To study the

						and experimental results.	influence of design factors on the heat exchange rate.
	Go et al. [31, 41]	Spiral-coil GHE	1) Soil region is regarded as a porous medium including the solid particles and pores; 2) Fluid region is treated as 1D model 3) The soil properties are regarded as constant values at all depths and temperatures.	1) The initial soil temperature and fluid velocity are 15.2 °C and 0.5m/s, respectively; 2) The calculation domain boundary 3D model is set as 30 m×15m×5m; 3) The inlet pipe wall temperature is regarded as the ground surface temperature.	Based on the FEM coupled with CFD analysis.	The mean difference is 3.92%, while the maximum difference is 8.85%.	1) To assess the influence of key input parameters on the system performance; 2) To provide an optimum design condition for the horizontal GHP unit; 3) To analyse the capital cost and payback time.
	Dasare and Saha [16]	Linear-loop, slinky-coil, and spiral-coil GHEs	1) The influence of acceleration is ignored; 2) No slip boundary conditions at the walls.	1) The initial condition is treated as the inlet fluid temperature: $T(x, y, H, t = 0) = \pm 7°C$; 2) The 3D calculation domain of size is defined as 2 m×2m×1.5m;	Based on the CFD analysis.	The discrepancy is less than 10% between 3D model and test data.	1) To investigate the thermal performance of different types of horizontal GHEs; 2) To analyse the effects of different factors on the heat transfer rate.
	Han et al. [43]	Linear-loop, slinky-coil, and spiral-coil GHEs	1) The working fluid flow is simplified as 1D model; 2) The heat transfer in the cross-section of working fluid inside the pipe is ignored;	1) The original inlet temperature is assumed as 6 °C; 2) The original soil temperature is also assumed as 6 °C; 3) The computational domain is assumed to be 35 × 32 × 10 m; 4) The GHE pipes are thought to be buried with the mean depth of 1.5 m underneath the soil surface; 5) The side and bottom boundaries of the soil region are defined as the Dirichlet boundary condition ; 6) The top of soil surface boundary is set as the Robin boundary condition;	Based on the COMSOL Multiphysics.	N/A	1) To study the heat transfer rate among the different horizontal GHEs; 2) To analyse the seasonal soil properties variation; 3) To assess the annual system performance.
	Selamat et al. [44]	Linear-loop, slinky-coil, and spiral-coil GHEs	1) The influence of soil temperature on the far-field boundaries is ignored; 2) The influence of groundwater movement, rain infiltration and contact thermal resistance are not taken into account.	1) All side walls are assumed as adiabatic boundaries; 2) The bottom boundary is defined as a constant heat flux of 65 W/m^2.	Based on the CFD analysis.	The difference is in the range from 1°C to 2°C.	1) To optimize the designs for horizontal GHEs based on various arrangements and pipe wall materials; 2) To assess the heat exchange rate of GHEs.

493

3.2 Economic evaluation approaches

Over the past few years, there has been an increasing number of articles which report on the cost of the horizontal GHP and compare with the conventional air-conditioning system. In this section, some economic indicators and feasibility solutions are reviewed. The horizontal GHP has substantially higher capital cost than the conventional air-conditioning system, mostly because of the initial expenses of heat pump and ground trench excavation work which take up almost 60% of the total construction expense. However, the horizontal GHP has low operational expense because of its high efficiency. Many economic indicators and methods are used to investigate the GHP initial cost, investment on return and payback period, including Levelized Cost of Heat (LCOH), Levelized Cost of Service (LCOS) , Capital Recovery Factor (CRF), Present Worth (PW) , Discounted Cash Flow Analysis (DCFA) , Internal Rate of Return (IRR) , Discounted Payback Period (DPP) , Simple Payback Period (SPP) , regression model and "NPV/operating duration" methods. These approaches are demonstrated in detail in the following section.

3.2.1 LCOH approach

Wang [45] adopted the levelized cost of heat (LCOH) approach to fulfil heat requirements for various domestic buildings. Three categories of heating technology are investigated and compared, including an air source heat pump (ASHP), a gas boiler and a GHP. This approach is given as:

$$\mathrm{LCOH} = \frac{\sum[\frac{\mathrm{Capital_t} + \mathrm{O\,\&\,M_t} + \mathrm{Fuel_t} + \mathrm{Carbon_t}}{(1+\mathrm{r})^t}]}{\sum[\frac{\mathrm{MWh_t}}{(1+\mathrm{r})^t}]} \quad (46)$$

where $\mathrm{Capital_t}$ is the capital expenditure in the year t (£); $\mathrm{O\&M_t}$ is the operation and maintenance expenses (£); $\mathrm{Fuel_t}$ and $\mathrm{Carbon_t}$ are the fuel and carbon costs in the year t (£), respectively; $(1 + r)_t$ is the discount factor in the year t with the discount rate r (%); $\mathrm{MWh_t}$ is the heat generated (MWh).

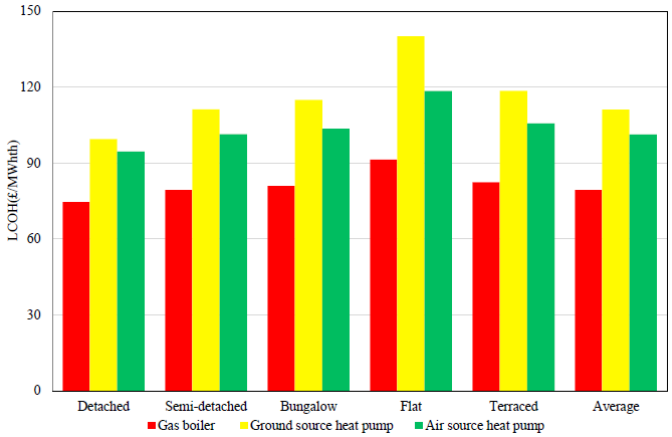

Fig. 41. The LCOH for gas boiler, ASHP and GHP for different dwelling categories [45]

Fig. 41 shows the LCOH results for five categories of domestic building with the average heating load. It is found that a gas boiler is the cheapest method to fulfil the heating requirements in all houses, with an overall LCOH of £75/MWh in a detached

house and just over £90/MWh in a flat. By comparison, a GHP system is the most expensive facility for fulfilling heating requirements in all dwelling categories. Furthermore, the LCOH for a flat is the highest because of its low yearly heat need reaching £140/MWh, roughly 20% higher than the ASHP and 30% higher than the GHP.

Welsch et al. [46] analysed the GHP by the LCOH method and presented:

$$\mathrm{LCOH} = \frac{\sum_{a=0}^{a_{end}} (I_a + M_a + F_a - R_a) \cdot (1+r)^{-a}}{\sum_{a=0}^{a_{end}} Q_a \cdot (1+r)^{-a}} \times 100 \tag{47}$$

where a_{end} is the over the assumed valuation period; I is the investment cost (£); M is the maintenance cost (£); F is the operating costs for fuel and electricity (£); r is the interest rate (%); Q is the system's discounted thermal energy output (kW).

Their results indicate that the energy expense, capital cost and interest rate are sensitive to the LCOH variation.

Daniilidis et al. [47] integrated the Ex-Post and Ex-Ante criteria to assess the financial cost of a GHP in Netherlands through the LCOH, NPV and Expected Monetary Value (EMV). The basic economic assessment method is written as:

$$\mathrm{LCOH} = \frac{\sum_{t=1}^{n} \frac{\mathrm{CapEx}_t + \mathrm{OpEx}_t}{(1+r)^t}}{\sum_{t=1}^{n} \frac{\mathrm{Heat}}{(1+r)^t}} \tag{48}$$

where CapEx is the capital cost in year t (£); r is the discount rate (%); OpEx is the operation expense in year t (£); Heat is the produced energy in year t (kW).

$$\mathrm{NPV} = \sum_{t=0}^{n} \frac{\mathrm{CF}_t}{(1+r)^t} \tag{49}$$

where CF is the net cash flow; t is the year.

The Expected Monetary Value (EMV) is defined as [47]:

$$\mathrm{EMV} = \mathrm{POS} \cdot \mathrm{NPV} + (1 - \mathrm{POS}) \cdot \mathrm{COF} \tag{50}$$

where POS is the Probability of Success for the doublet drilling; COF is the Costs of Failure which are the monetary values for a successful and a failed doublet drilling, respectively.

According to Fig. 42, it can be found that the drilling and piping system deployment expenses are the major initial disbursements, however, the sensitivity discloses that the NPV is mostly affected by the gas saturation and flow rate. The LCOH indicatrix is mainly sensitive to geological parameters including permeability and depletion, operational parameters including injection temperature and load factor as well as technical inputs parameters including network length and expense, the efficiency of heat exchanger [47].

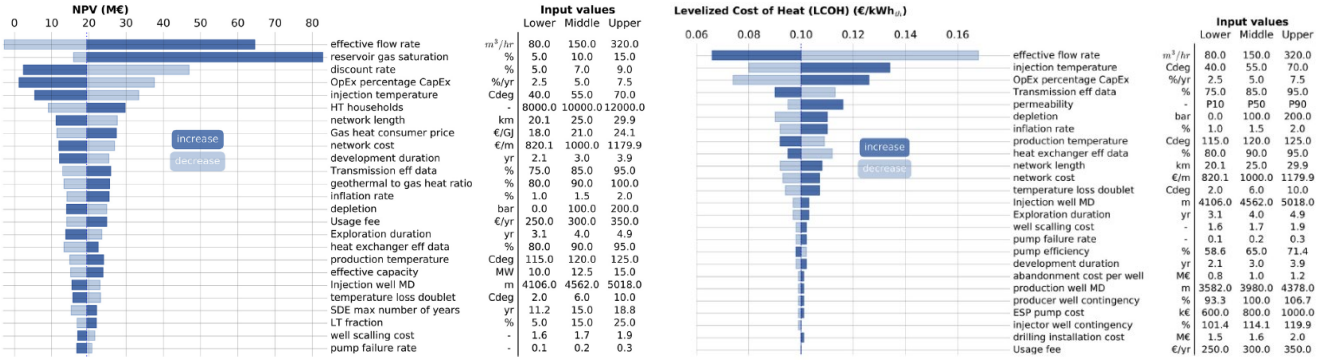

Fig. 42. Sensitivity analysis for: (a) NPV index; (b) LCOH index [47]

3.2.2 LCOS approach

Wiryadinata et al. [48] utilized the levelized cost of service (LCOS) approach to analyse the potential benefits of the GHP for the low-rise lodging and multifamily facilities in USA. The LCOS is expressed as:

$$\mathrm{LCOS} = \{\frac{\sum_y[(\mathrm{P_y})\cdot \mathrm{n}(1+\mathrm{n})^{\mathrm{M}}]}{[(1+\mathrm{n})^{\mathrm{M}}-1][\sum_{\mathrm{j}=1}^{20}\sum_{\mathrm{i}=1}^{8760}(\mathrm{CL_i}+\mathrm{HL_i})_{\mathrm{j}}]}\} \quad (51)$$

$$\mathrm{P_y} = \sum_{\mathrm{j}=1}^{20}\mathrm{Co_y}[\frac{(1+\mathrm{s_y})}{(1+\mathrm{n})}]^{\mathrm{j}} \quad (52)$$

where P is the NPV over their lifetime ($); Co is the expense at the first year ($); n is the yearly interest (%); s is the annual price escalation rate (%); M is 20 years; y is the different element of total expense ($).

It is indicated that the energy LCOS savings are lower than the maintenance LCOS savings. Specifically, the total LCOS savings, which are evaluated to become between \$1.7/m^2/year and \$3.6/m^2/year, are affected by a mass of assumption conditions. The GHP initial cost is the most sensitive to installation expense and system efficiency.

3.2.3 PW approach

Present worth (PW) is also known as the present value (PV), which is the current value of a future sum of money or stream of cash flows given a specified rate of return. Noorollahi et al. [33] investigated the economic benefits of the GHP for a greenhouse in Iran by the PW method.

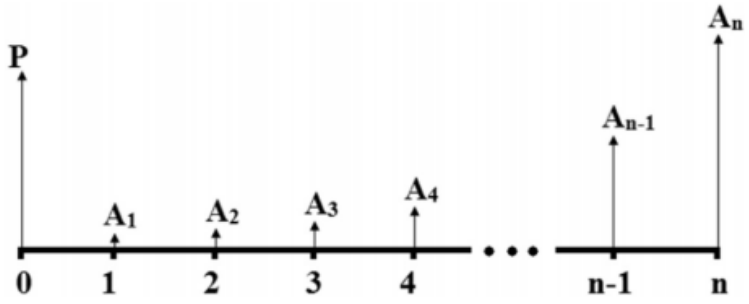

Fig. 43. Cash flow diagram of projects [33]

558 It can be seen from Fig. 43 that the cash flow diagram contains a capital expense (P) and an operation expense in the first year
559 (A1) inflated by the rate of j in the next year.
560 The PW of the cash flow is expressed as:

561 $$PW = P + A_1[\frac{1-(\frac{1+j}{1+i})^n}{i-j}] \quad (53)$$

562 where P is the initial expense; A1 is the operating expense in the first year; i is the minimum attractive rate of return; j is the
563 inflation rate (%).
564 Four different inflation rates of 15%, 20%, 25%, and 30% are compared to obtain the most economical solution. It is denoted
565 that the GHP with five heat pumps and 2500 m GHE is the most economically attractive among all GHP projects for 30 years of
566 operation.
567 Hakkaki-Fard et al. [49] performed a LCC assessment to study the difference between the capital and 10-year operation expenses
568 of the ASHP and GHP by means of the PW method in Canada. The PW is written as:

569 $$PW_{electricity} = \frac{COST_{annual}}{(1+ESC)^{year}} \cdot (1+DISC)^{year} \quad (54)$$

570 where $COST_{annual}$ is the annual electricity expense (£); DISC is the real Montreal discount rate (%); ESC is the electricity
571 escalation rate (%).
572 The total cost is given as:

573 $$LCC = IC + PW_{electricity} \quad (55)$$

574 where IC is the capital investment of heat pump at year 0.
575 It is found that the payback period of the GHP is more than 15 years. Nevertheless, the payback period would be fallen to just a
576 few years if the GHE installation price is decreased by 50%.
577 3.2.4 IRR approach
578 Internal rate of return (IRR) method also considers the time value of money. It is used to study an investment project by
579 comparing the internal rate of return to the minimum required rate of return of the project [50]. Morrone et al. [50] implemented
580 the financial analyses of energy pile systems over 20 years of operation in Naples and Milan, Italy. The main economic indicators
581 including the NPV, IRR and Profitability Index (PI) are given as:

582 $$\sum_{k=1}^{DPB} S_k(1+i)^{-k} = OC \quad (56)$$

583 $$NPV = \sum_{k=1}^{N-1} S_k(1+i)^{-k} - OC \quad (57)$$

$$0 = \sum_{k=1}^{N-1} S_k (1 + IRR)^{-k} - OC \quad (58)$$

$$PI = \frac{NPV}{OC} \quad (59)$$

where S_k is the economical saving per annum (€/year); OC is the whole expense of the alternative system to the conventional one (€); i is the yearly discount rate (%).

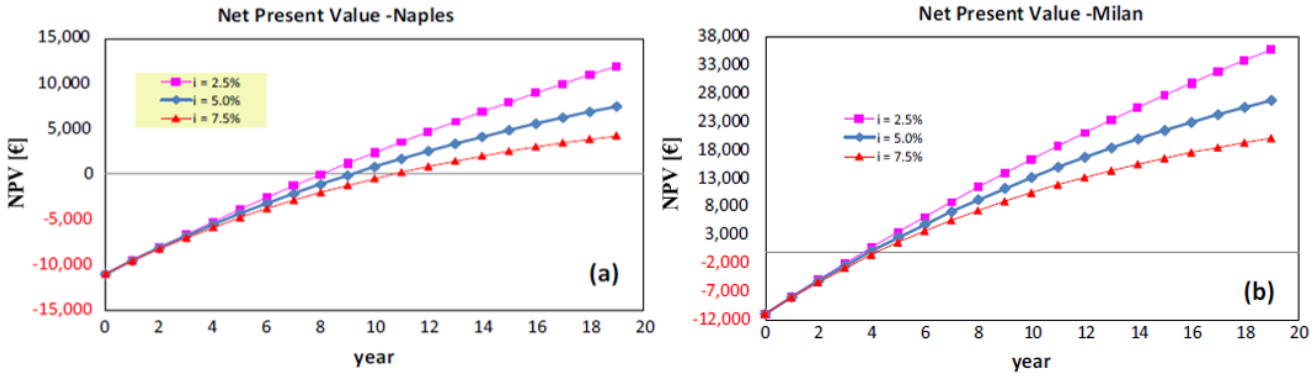

Fig. 44. NPV variation with time at different interest rates: (a) Naples; (b) Milan [50]

Fig. 44 presents the yearly savings of the horizontal GHP at different discount rates of 2.5%, 5% and 7.5% in Naples and Milan for 20 years' operation. The NPV trend in Naples is similar to the one in Milan, but the economic performance in Milan is much better than that in Naples. Specifically, in Milan, the PI is 243% in terms of a discount rate of 5%, which stands for a wonderful economic performance, and the IRR shows a high value of 28.2%, by contrast in Naples, the PI of the investment with a discount rate of 5% is around 70%, which indicates the IRR index is equivalent to 12.4% displaying that the margin of revenue is quite limited [50].

Ghoreishi-Madiseh and Kuyuk [51] implemented an economic analysis of the GHP by means of the NPV and IRR methods. The NPV is written as:

$$NPV = \sum_{t=0}^{n} \frac{CF_t}{(1 + IRR)^t} \quad (60)$$

where CF_t is the cash flow at time t (£); IRR is the interest rate (%); n is the years of operation (year).

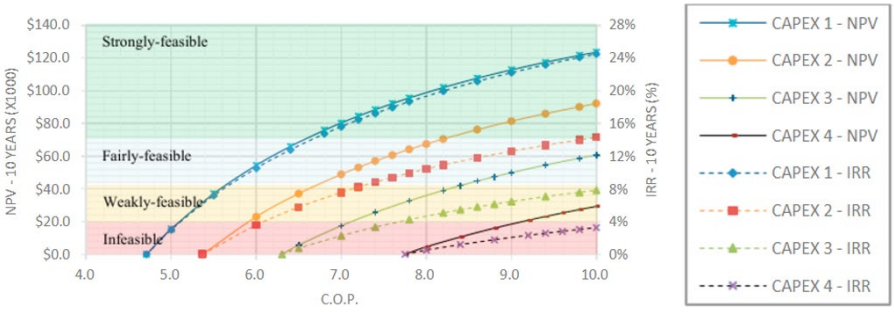

Fig. 45. Effect of COP on IRR and NPV [51]

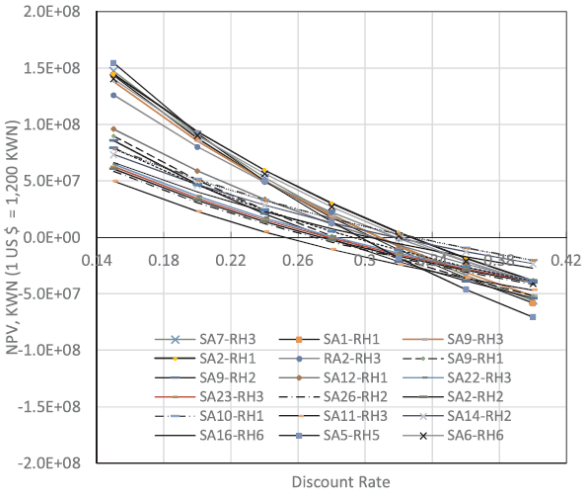

Fig. 46. NPV variation with discount rate for IRR assessment [52]

Fig. 45 describes the influences of heat pump COP on the IRR and NPV values. The IRR is largely a discount rate that brings the NPV to zero, thereby the IRR is able to be calculated by an NPV versus discount rate curve as shown in Fig. 46 [52]. These results conclude that the predictable growth rates that vary from 25.6% to 33.5% are higher than the said discount rate (15%), which discloses the proposed deployment scheme of the GHP should be quite attractive in terms of the investment perspective.

3.2.5 DCFA approach

Gabrielli and Bottarelli et al. [53] compared the economic benefits of the GHP versus traditional condensing boiler (CB) to attain the cost-benefit analysis (CBA) based on the discounted cash flow analysis (DCFA).

The cost of investment C_i is determined as:

$$C_i = C_0 + \sum_{t=0}^{n} C_0 \cdot [(\frac{r}{(1+r)^t - 1}) \cdot \frac{1}{(1+r)^t}] \quad (61)$$

where C_0 is the instalment cost (£); r is the discount rate (%).

The operating cost is given as:

$$Ce = \sum_{t=0}^{n} C_E \cdot [\frac{(1+g)^t}{(1+r)^t}] \quad (62)$$

where Ce is the operating expenses (£); g is the increasing rate (%).

3.2.6 SPP approach

The simple payback period (SPP) is the span of time needed to recover the expense of a capital investment. However, the SPP overlooks the time value of money.

$$SPP = \frac{\text{Initial investment made}}{\text{Net annual cash inflow}} \quad (63)$$

Ren et al. [54] assessed the financial benefits of the GHP with both polyethylene and steel heat exchangers in China, and indicated that the payback periods of the polyethylene and steel heat exchangers are individual 3.45 years and 1.83 years, based on the SPP method. Kharseh et al. [55] assessed a GHP as a heating, ventilation, and air conditioning (HVAC) unit for a domestic building in Qatar, and denoted that the SPP is about 9 years, whereas for similar application in Melbourne the SPP is 4.24 years [56].

3.2.7 DPP approach

The discounted payback period (DPP) method is a capital budgeting process to regulate the profitability of a project. The basic equation is expressed as below:

$$\mathrm{DPP} = \text{Year before the DPP occurs} + \frac{\text{Cumulative cash flow in year before recovery}}{\text{Discounted cash flow in year after recovery}} \tag{64}$$

Gabrielli and Bottarelli [53] studied the DPP for a domestic building in Italy given as:

$$\mathrm{DPP} = \frac{C_{0GHP} + \sum_{t=0}^{n} C_0[(\frac{r}{q^t - 1}) \cdot \frac{1}{q^t}] - C_0 + \sum_{t=0}^{n} C_{0CB}[(\frac{r}{q^t - 1}) \cdot \frac{1}{q^t}]}{\sum_{t=0}^{n} C_{ECB}[\frac{(1+g)^t}{q^t}] - \sum_{t=0}^{n} C_{EGHP}[\frac{(1+g)^t}{q^t}]} \tag{65}$$

where C_{0GHP} is the investment expense for the GHP (£); C_{0CB} is the investment expense for traditional condensing boiler (£); C_{EGHP} is the operating cost for the GHP (£); C_{ECB} is the operating cost for the CB (£).

Their results denote that when the PBP is lower than some predicted number of years (15 years), the initial cost of the GHP is worthy undertaking. Morrone et al. [50] compared the payback times of the GHP in Naples and Milan by using the DPP method, and illustrated that the GHP cost-saving can be attained about 20% with 8-11 years' DPP compared to the traditional system in Naples, by contrast, the energy-saving is assessed not more than 10% with 4 years' DPP in Milan. Imal et al. [57] performed the payback time analysis of a GHP for a 25 years' lifetime, and obtained that the GHP saves $791/year with 8 years of payback period as presented in Fig. 47.

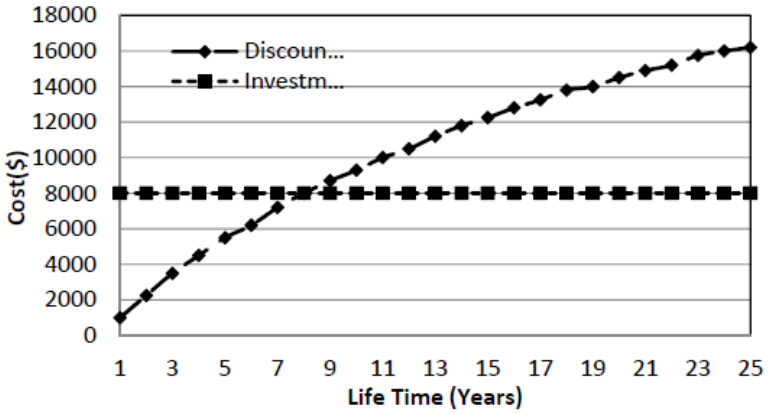

Fig. 47. PW variation with DPP [57]

3.2.8 Other approaches

Yousefi et al. [10] proposed a regression model to predict the annual expense based on the ambient temperature and building cooling/heating loads in Iran. The equation is given as:

$$Y = 7.32X_1 + 117.13X_2 - 1840.26 \quad (66)$$

where Y is the yearly expense (£); X_1 is the temperature (K); X_2 is the cooling/heating ratio (%).

It can be found from Fig. 48 that the cooling/heating demand ratio varies from 0.66 to 3.45, and the cooling/heating ratio can be utilized to forecast the yearly expense.

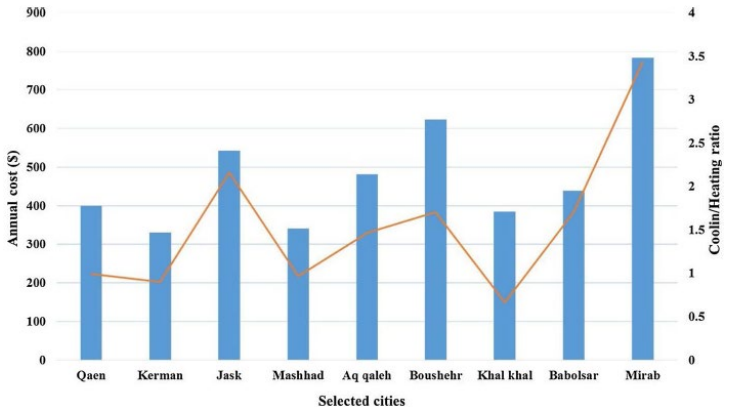

Fig. 48. A comparison between energy ratio and total annual system expense [10]

Kayaci and Demir [58] utilized the capital recovery factor (CRF) method to do the economic analysis in Turkey. The annual amount (A) is calculated by using the CRF at a constant interest rate expressed as:

$$A = (C_i + C_e) \cdot CRF \quad (67)$$

where C_i is the initial cost (£); C_e is the energy cost of the system (£); CRF is utilized to allocate a single amount invested today over a uniform series of end year payment. The equations are obtained as follows:

$$C_i = C_{pipe} + C_{earthwork} + C_{heatpump} + C_{circulationpump} + C_{labor} \quad (68)$$

$$C_e = C_{e,1} + \sum_{n=2}^{n=10} C_{e,n} e \quad (69)$$

$$CRF = [\frac{i(i+1)^{\upsilon}}{(i+1)^{\upsilon} - 1}] \quad (70)$$

where i is the interest rate (%); υ is the year of payback period (year).

Nguyen et al. [59] performed an economic analysis for a fast food restaurant (NPV) by a new variable "NPV/operating duration" method. Fig. 49 displays the annual NPV variation in the operating period. The yearly system expense decreases with the operating duration, this reflects the fact that the initial investment is spread over a longer timeframe. Thereby, the fast food restaurant NPV cost per annum levels off after very long duration of operation.

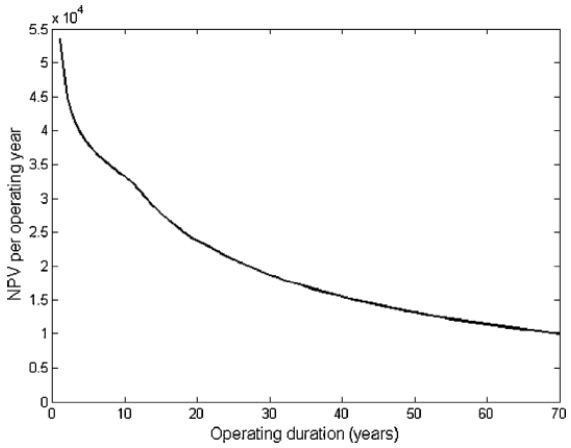

664

665 **Fig. 49.** Variation of NPV per annum with operating time for a fast food restaurant [59]

666 3.2.9 Comparison of economic evaluation methods

667 A number of economic approaches have been utilized extensively to evaluate the financial factors which impact the market for
668 the horizontal GHPs in different countries. According to these research results, it can be found for the horizontal GHP that: 1)
669 the NPV is about £24000–£30000 for a 20–30 years' service lifetime; 2) the payback period is in the range of 4 to10 years on
670 the whole. Apart from the variety of economic indicators, there is often a remarkable discrepancy in the economic impact factors
671 such as time and location, inflation and discount rates, fuel expense, mortgage interest, electricity tariff as well as incentives,
672 which could lead to substantial differences in the key financial performance and investment decision. Hence, a comparison of all
673 proposed economic models is presented in Table 8**.**

674 **Table 8** Comparison of economic models

Model name	Impact factors													
	System energy generation	**Annual costs**	**Initial costs**	**O&M costs**	**Fuel costs**	**Carbon costs**	**Replacement cost**	**Discount rate**	**Interest rate**	**Inflation rate**	**Time value of money**	**Net cash flow**	**Discounted cash flow**	**Heating/ cooling ratio**
Regression model [10]	✓	✓	✗	✗	✗	✗	✗	✗	✗	✗	✗	✗	✗	✓
LCOH [45-47]	✓	✓	✓	✓	✓	✓	✗	✓	✓	✗	✓	✓	✓	✗
LCOS [48]	✓	✓	✓	✓	✗	✗	✗	✗	✓	✗	✓	✓	✗	✗
CRF [58]	✓	✓	✓	✓	✗	✗	✗	✗	✓	✗	✗	✓	✗	✗
PW [33, 49]	✓	✓	✓	✓	✗	✗	✗	✗	✓	✓	✓	✓	✗	✗
IRR [50, 51]	✓	✓	✓	✓	✗	✗	✗	✓	✗	✗	✓	✗	✓	✗
DCFA [53]	✓	✓	✓	✓	✗	✗	✗	✓	✗	✗	✓	✗	✓	✗
DPP [50, 53, 57]	✗	✓	✓	✓	✗	✗	✗	✓	✗	✗	✓	✗	✓	✗
SPP [54-56]	✗	✓	✓	✓	✗	✗	✓	✗	✓	✗	✗	✓	✗	✗
NPV/operating duration [59]	✓	✓	✓	✓	✗	✗	✓	✗	✓	✓	✗	✓	✗	✗

675

4. Critical observations and recommendations for future study

The techno-economic assessment of the horizontal GHP is an imperatively challenging area of research. The analytical and numerical models are combined as a useful tool to predict the working fluid temperature, heat transfer rates within a GHE, system performance and energy output. Additionally, some methods are also necessary to assess the financial benefits of the horizontal GHP. Yet, some techno-economic models of the horizontal GHP have been generalized in detail.

Most analytical models are established based on the principle of superposition, thermal resistance, mirror image and Green's function methods, in which the temperatures of the GHE and neighbouring ground are determined through a series of temperature nodes. Many amendments have been put forward on the analytical models, normally by adding a point heat source, and dividing the GHE into two or more regions. Nevertheless, when a high accuracy is required, more nodes are needed to be supplied, leading to massive of formulations that must be resolved properly to satisfy for accuracy requirement. Owing to a mass of differential equation requisites for a proper discretization in the GHE, several models are limited to the analytical type. Numerical methods are more accurate and dynamic, and performed by using the innovative methodologies and have been applied in the recent years. Meanwhile, the numerical models permit any category of geometry and conduce to determining the soil temperature within the GHE. On the other side, the numerical methods have the ability to assess the transient refrigerant flow along the pipe. The effects of the ground thermal conductivity, refrigerant flow rate, GHE depth and pitch spacing on the outlet refrigerant temperature, thermal short-circuiting loss and mean heat exchange rate can also be clarified.

Most economic feasibility assessments conducted for the horizontal GHP adopt a number of simple economic approaches, such as LCOH, IRR, PW, and SPP. More advanced approaches such as LCOS, regression model, CRF,NPV/operating duration, DCFA and DPP are also utilized. The merit of the advanced economic approaches is considering all future costs. These methods offer the assessment of future expenses with today's expenses. On the other hand, the cash flow considers the time value of money and future inflation rate.

Although more efforts have been focussed on the application and enhancement of the techno-economic assessments, there are still a few domains that require to be given attention to create the framework for forthcoming study in order to spread out the applicability of the horizontal GHP technology, those domains are summarized in the following:

- A number of existing analytical and numerical methods have not taken into account the influence of the moisture on the performance of the horizontal GHE, where the groundwater advection is sensitive to the depth, number and spacing of the GHEs. More researches should be focused on this aspect.
- To decrease the installation expense and promote the horizontal GHP technology, the minimum required length of GHE needs to be precisely deduced through analytical or numerical approach. The possibility of further reducing trench size by using smaller loop slinky coil and its effect on thermal performance should be investigated.

- The dynamic ground surface temperature cannot be presumed as an adiabatic boundary value or a constant value because of the complicated processes and mutual effects including the influences of cloud cover, solar radiation, relative humidity, ambient temperature, rainfall, wind speed, surface reflectivity as well as snow cover and so on.

5. Conclusions

The GHP system, which makes use of the soil as the heat source or sink, has high energy efficiency and low carbon emission. Despite its merits, the comparatively high capital expense is still an obstacle preventing the application of the vertical GHP technology. In comparison, the horizontal GHP system, which is mounted in a shallow trench with linear-loop, or slinky-coil or spiral-coil GHE, is a cost-effective option as the excavation expense of the horizontal trenches is prominently lower than the drilling expense of the vertical GHE. It is necessary to review various horizontal GHE options, typically in terms of system energy generation, economic and environmental benefits. Some important outcomes are obtained as follows:

1) Heat transfer models of different horizontal GHE geometric structures are generalized including the linear-loop, slinky-coil and spiral-coil types. The spiral-coil GHE exhibits a better performance in the light of heat exchange rate compared to the linear-loop and slinky-coil types. Moreover, the soil thermal conductivity and working fluid flow rate within the pipe play important roles on heat transfer for the horizontal GHE arrangement but the installation depth of the horizontal GHE has weak influence.
2) Most analytical models are developed on the basis of the principle of superposition, line source model, thermal resistance theory, Green's function and mirror image methods. The heat transfer mechanism is usually treated under the steady-state and determined through a sequence of temperature nodes. Although analytical models need less calculating time, they are weak for high precision simulation with a long-term operation. To solve the issue, several numerical models are established by the FEM, FDM, FVM, ADI with some commercial software including the CFD, Matlab, FEFLOW and COMSOL due to more accurate nature. Numerical models consider the effects of the soil thermal conductivity, working fluid flow rate, thermal short-circuiting between the pitch spacing and ground surface. However, the main drawback of numerical approaches is their long computation periods in terms of the complex heat transfer and discretization procedures.
3) Most economic analyses for the horizontal GHP system use a number of simple approaches like LCOH, IRR, PW, and SPP methods. More innovative approaches such as LCOS, regression model, CRF, NPV/operating duration, DCFA and DPP methods are rarely employed. The advantage of using the advanced economic approaches is considering all future costs and economic parameter variations, the cash flow is determined by the time value of money and future inflation rate.
4) For future investigations, the computer programs should be further established, and a comprehensive evaluation is definitely needed to proof their precisions for the practical applications. Moreover, for the horizontal GHP system, the minimum pipe length is needed to be precisely decided through analytical or numerical approaches for research and engineering practices.

736 **References**

737 [1] Aresti A, Christodoulides P, Florides G. A review of the design aspects of ground heat exchangers. Renewable and
738 Sustainable Energy Reviews 2018; 92: 757–773.

739 [2] Alkaff SA, Sim SC, Ervina EMN. A review of underground building towards thermal energy efficiency and sustainable
740 development. Renewable and Sustainable Energy Reviews 2016; 60: 692–713.

741 [3] Bel G, Joseph S. Climate change mitigation and the role of technological change: Impact on selected headline targets of
742 Europe's 2020 climate and energy package. Renewable and Sustainable Energy Reviews 2018; 82; 3798-3807.

743 [4] Sansaniwal SK, Sharma V, Mathur J. Energy and exergy analyses of various typical solar energy applications: A
744 comprehensive review. Renewable and Sustainable Energy Reviews 2018; 82: 1576-1601.

745 [5] Sahu BK. Wind energy developments and policies in China: A short review. Renewable and Sustainable Energy Reviews
746 2018; 81: 1393-1405.

747 [6] Bai Z, Liu Q, Lei J, Wang X, Sun J, Jin H. Thermodynamic evaluation of a novel solar-biomass hybrid power generation
748 system. Energy Conversion and Management 2017; 142: 296-306.

749 [7] Cui Y, Zhu J, Twaha S, Riffat S. A comprehensive review on 2D and 3D models of vertical ground heat exchangers.
750 Renewable and Sustainable Energy Reviews 2018; 94: 84-114.

751 [8] Li C, Mao J, Peng X, Mao W, Xing Z, Wang B. Influence of ground surface boundary conditions on horizontal ground source
752 heat pump systems, Applied Thermal Engineering 2019; 152: 160-168.

753 [9] Ghoreishi-Madiseh SA, Kuyuk AF, Brito MAR.An analytical model for transient heat transfer in ground-coupled heat
754 exchangers of closed-loop geothermal systems. Applied Thermal Engineering 2019; 150: 696-705.

755 [10] Yousefi H, Ármannsson H, Roumi S, Tabasi S, Mansoori H, Hosseinzadeh M. Feasibility study and economical evaluations
756 of geothermal heat pumps in Iran. Geothermics 2018; 72: 64-73.

757 [11] Makasis N, Narsilio GA, Bidarmaghz A, Johnston IW. Ground-source heat pump systems: The effect of variable pipe
758 separation in ground heat exchangers. Computers and Geotechnics 2018; 100: 97-109.

759 [12] Lu Q, Narsilio GA, Aditya GR, Johnston IW. Economic analysis of vertical ground source heat pump systems in Melbourne.
760 Energy 2017; 125:107-117.

761 [13] Jeon JS, Lee SR, Kim MJ. A modified mathematical model for spiral coil-type horizontal ground heat exchangers. Energy
762 2018; 152: 732-743.

763 [14] Athresh AP, Al-Habaibeh A, Parker K. The design and evaluation of an open loop ground source heat pump operating in
764 an ochre-rich coal mine water environment. International Journal of Coal Geology 2016; 164: 69–76.

765 [15] Javadi H, Ajarostaghi SSM, Pourfallah M, Zaboli M. Performance analysis of helical ground heat exchangers with different
766 configurations. Applied Thermal Engineering 2019; 154: 24-36.
767 [16] Dasare RR, Saha SK. Numerical study of horizontal ground heat exchanger for high energy demand applications. Applied
768 Thermal Engineering 2015; 85: 252-263.
769 [17] Neupauer K, Pater S, Kupiec K. Study of ground heat exchangers in the form of parallel horizontal pipes embedded in the
770 ground. Energies 2018; 11 (3): 491.
771 [18] Kupiec K, Larwa B, Gwadera M. Heat transfer in horizontal ground heat exchangers. Applied Thermal Engineering 2015;
772 75: 270-276.
773 [19] Li C, Mao J, Peng X, Mao W, Xing Z, Wang B. Influence of ground surface boundary conditions on horizontal ground
774 source heat pump systems, Applied Thermal Engineering 2019; 152: 160-168.
775 [20] Pu L, Xu L, Qi D, Li Y. Structure optimization for horizontal ground heat exchanger. Applied Thermal Engineering 2018;
776 136: 131-140.
777 [21] Rees SJ. Horizontal and compact ground heat exchangers. Advances in Ground-Source Heat Pump Systems, Woodhead
778 Publishing, Pages 117-156, 2016.
779 [22] Zukowski M, Topolanska J. Comparison of thermal performance between tube and plate ground-air heat exchangers.
780 Renewable Energy 2018; 115: 697-710.
781 [23] Lund JW, Boyd TL. Direct utilization of geothermal energy 2015 worldwide review. Geothermics 2016; 60: 66–93.
782 [24] Aydin M, Sisman A, Gultekin A, Dehghan B. An experimental and computational performance comparison between
783 different shallow ground heat exchangers. Proceedings World Geothermal Congress 2015 Melbourne, Australia, 19-25
784 April 2015. Available at < https://pangea.stanford.edu/ERE/db/WGC/papers/WGC/2015/29058.pdf > Access [04. 2015].
785 [25] Selamat SB. Numerical modelling for horizontal ground heat exchangers optimization. Department of science and advanced
786 technology graduate school of science and engineering Saga University, Japan. Available at <http://portal.dl.saga-
787 u.ac.jp/bitstream/123456789/122573/4/zenbun_fulltext_salsuwanda.pdf > Access [03. 2016].
788 [26] Xiong Z, Fisher DE, Spitler JD. Development and validation of a Slinky™ ground heat exchanger model. Applied Energy
789 2015; 141: 57-69.
790 [27] Lee JU, Kim T, Leigh SB. Applications of building-integrated coil-type ground-coupled heat exchangers—Comparison of
791 performances of vertical and horizontal installations. Energy and Buildings 2015; 93: 99-109.
792 [28] Yoon S, Lee SR, Go GH. Evaluation of thermal efficiency in different types of horizontal ground heat exchangers. Energy
793 and Buildings 2015; 105:100–105.

794 [29] Kim MJ, Lee SR, Yoon S, Jeon JS. An applicable design method for horizontal spiral-coil-type ground heat exchangers.
795 Geothermics 2018; 72: 338-347.
796 [30] Wang De, Lu L, Cui P. A new analytical solution for horizontal geothermal heat exchangers with vertical spiral coils.
797 International Journal of Heat and Mass Transfer 2016; 100: 111-120.
798 [31] Go GH, Lee SR, Yoon S, Kim MJ. Optimum design of horizontal ground-coupled heat pump systems using spiral-coil-loop
799 heat exchangers. Applied Energy 2016; 162: 330-345.
800 [32] Kim MJ, Lee SR, Yoon S, Jeon JS. Evaluation of geometric factors influencing thermal performance of horizontal spiral-
801 coil ground heat exchangers. Applied Thermal Engineering 2018; 144: 788-796.
802 [33] Noorollahi Y, Bigdelou P, Pourfayaz F, Yousefi H. Numerical modeling and economic analysis of a ground source heat
803 pump for supplying energy for a greenhouse in Alborz province, Iran. Journal of Cleaner Production 2016; 131: 145-154.
804 [34] Todoran TP, Balan MC. Long term behavior of a geothermal heat pump with oversized horizontal collector. Energy and
805 Buildings 2016; 133: 799-809.
806 [35] Sofyan SE, Hu E, Kotousov A. A new approach to modelling of a horizontal geo-heat exchanger with an internal source
807 term. Applied Energy 2016; 164: 963-971.
808 [36] Kayaci N, Demir H. Numerical modelling of transient soil temperature distribution for horizontal ground heat exchanger of
809 ground source heat pump. Geothermics 2018; 73: 33–47.
810 [37] Sangi R, Müller D. Dynamic modelling and simulation of a slinky-coil horizontal ground heat exchanger using Modelica.
811 Journal of Building Engineering 2018; 16: 159–168.
812 [38] Li H, Nagano K, Lai Y. Heat transfer of a horizontal spiral heat exchanger under groundwater advection. International
813 Journal Heat Mass Transfer 2012; 55: 6819–6831.
814 [39] Li C, Mao J, Zhang H, Xing Z, Li Y, Zhou J. Numerical simulation of horizontal spiral-coil ground source heat pump system:
815 Sensitivity analysis and operation characteristics. Applied Thermal Engineering 2017; 110: 424-435.
816 [40] Kim MJ, Lee SR, Yoon S, Go GH. Thermal performance evaluation and parametric study of a horizontal ground heat
817 exchanger. Geothermics 2016; 60: 134-143.
818 [41] Go GH, Lee SR, Nikhil NV, Yoon S. A new performance evaluation algorithm for horizontal GCHPs (ground coupled heat
819 pump systems) that considers rainfall infiltration. Energy 2015; 83: 766-777.
820 [42] Habibi M, Hakkaki-Fard A. Evaluation and improvement of the thermal performance of different types of horizontal ground
821 heat exchangers based on techno-economic analysis. Energy Conversion and Management 2018; 171: 1177–1192.
822 [43] Han C, Ellett KM, Naylor S, Yu X. Influence of local geological data on the performance of horizontal ground-coupled heat
823 pump system integrated with building thermal loads. Renewable Energy 2017; 113: 1046-1055.

824 [44] Selamat S, Miyara A, Kariya K. Numerical study of horizontal ground heat exchangers for design optimization. Renewable
825 Energy 2016; 95: 561-573.
826 [45] Wang Z. Heat pumps with district heating for the UK's domestic heating: individual versus district level. Energy Procedia
827 2018; 149: 354-362.
828 [46] Welsch B, Göllner-Völker L, chulte DO, Bär K, Sass I, Schebek L. Environmental and economic assessment of borehole
829 thermal energy storage in district heating systems. Applied Energy 2018; 216: 73-90.
830 [47] Daniilidis A, Alpsoy B, Herber R. Impact of technical and economic uncertainties on the economic performance of a deep
831 geothermal heat system. Renewable Energy 2017; 114: 805-816.
832 [48] Wiryadinata S, Modera M, Jenkins B, Kornbluth K. Technical and economic feasibility of unitary, horizontal ground-loop
833 geothermal heat pumps for space conditioning in selected California climate zones. Energy and Buildings 2016; 119: 164-
834 172.
835 [49] Hakkaki-Fard A, Eslami-Nejad P, Aidoun Z, Ouzzane M. A techno-economic comparison of a direct expansion ground-
836 source and an air-source heat pump system in Canadian cold climates. Energy 2015; 87: 49-59.
837 [50] Morrone B, Coppola G, Raucci V. Energy and economic savings using geothermal heat pumps in different climates. Energy
838 Conversion and Management 2014; 88: 189-198.
839 [51] Ghoreishi-Madiseh SA, Kuyuk AF. A techno-economic model for application of geothermal heat pump systems. Energy
840 Procedia 2017; 142: 2611-2616.
841 [52] Seo Y, Seo UJ, Kim JH. Economic feasibility of ground source heat pump system deployed in expressway service area.
842 Geothermics 2018; 76: 220–230.
843 [53] Gabrielli L, Bottarelli M. Financial and economic analysis for ground-coupled heat pumps using shallow ground heat
844 exchangers. Sustainable Cities and Society 2016; 20: 71–80.
845 [54] Ren C, Deng Y, Cao SJ. Evaluation of polyethylene and steel heat exchangers of ground source heat pump systems based
846 on seasonal performance comparison and life cycle assessment. Energy and Buildings 2018: 162: 54-64.
847 [55] Kharseh M, Al-Khawaja M, Suleiman MT. Potential of ground source heat pump systems in cooling-dominated
848 environments: residential buildings. Geothermics 2015; 57: 104–110.
849 [56] Lu Q, Narsilio GA, Aditya GR, Johnston IW. Economic analysis of vertical ground source heat pump systems in Melbourne.
850 Energy 2017; 125:107-117.
851 [57] Imal M, Yılmaz K, Pınarbaşı A. Energy efficiency evaluation and economic feasibility analysis of a geothermal heating and
852 cooling system with a vapor-compression chiller system. Sustainability 2015; 7: 12926-12946.

[58] Kayaci N, Demir H. Long time performance analysis of ground source heat pump for space heating and cooling applications based on thermo-economic optimization criteria. Energy and Buildings 2018; 163: 121-139.

[59] Nguyen HV, Law YLE, Zhou X, Walsh PR, Leong WH, Dworkin SB. A techno-economic analysis of heat-pump entering fluid temperatures, and CO2 emissions for hybrid ground-source heat pump systems. Geothermics 2016; 61: 24-34.